Received: 5 March 2024 | Revised: 30 May 2024 | Accepted: 7 June 2024

DOI: 10.1002/hyp.15211

RESEARCH ARTICLE

WILEY

Alignment between water inputs and vegetation green-up reduces next year's runoff efficiency

Sarah K. Newcomb[1] | Robert W. Van Kirk[2] | Sarah E. Godsey[1] | Maggi Kraft[1]

[1]Department of Geosciences, Idaho State University, Pocatello, Idaho, USA

[2]Henry's Fork Foundation, Ashton, Idaho, USA

Correspondence
Sarah K. Newcomb, Department of Geosciences, Idaho State University, Pocatello, ID, USA.
Email: sarahnewcomb@isu.edu

Funding information
National Science Foundation, Grant/Award Number: 1653998

Abstract

In the western United States, water supplies largely originate as snowmelt from forested land. Forests impact the water balance of these headwater streams, yet most predictive runoff models do not explicitly account for changing snow-vegetation dynamics. Here, we present a case study showing how warmer temperatures and changing forests in the Henrys Fork of the Snake River, a seasonally snow-covered headwater basin in the Greater Yellowstone Ecosystem, have altered the relationship between April 1st snow water equivalent (SWE) and summer streamflow. Since the onset and recovery of severe drought in the early 2000s, predictive models based on pre-drought relationships over-predict summer runoff in all three headwater tributaries of the Henrys Fork, despite minimal changes in precipitation or snow accumulation. Compared with the pre-drought period, late springs and summers (May–September) are warmer and vegetation is greener with denser forests due to recovery from multiple historical disturbances. Shifts in the alignment of snowmelt and energy availability due to warmer temperatures may reduce runoff efficiency by changing the amount of precipitation that goes to evapotranspiration versus runoff and recharge. To quantify the alignment between snowmelt and energy on a timeframe needed for predictive models, we propose a new metric, the Vegetation-Water Alignment Index (VWA), to characterize the synchrony of vegetation greenness and snowmelt and rain inputs. New predictive models show that in addition to April 1st SWE, the previous year's VWA and summer reference evapotranspiration are the most significant predictors of runoff in each watershed and provide more predictive power than traditionally used metrics. These results suggest that the timing of snowmelt relative to the start of the growing season affects not only annual partitioning of streamflow, but can also determine the groundwater storage state that dictates runoff efficiency the following spring.

KEYWORDS
antecedent moisture, drought, headwaters, runoff efficiency, seasonal runoff predictions, similarity index, vegetation greenness

1 | INTRODUCTION

1.1 | Predicting summer streamflow in seasonally snow-covered headwaters

Across the western United States, over half the water that annually replenishes rivers and reservoirs originates as snowmelt (Li et al., 2017). The timing and amount of snowmelt that becomes streamflow determines how much water will be available for irrigation, hydroelectric power generation and instream fish habitat (Barnett et al., 2005; Barnhart et al., 2016, 2020). Each year, irrigators and water managers rely on seasonal streamflow predictions issued in the spring that forecast summer water availability (Garen, 1992; Pagano et al., 2004). Many of these regression-based seasonal predictive models are founded on the relationship between April 1st snow water equivalent (SWE) and summer streamflow. Seasonal streamflow predictions are notoriously difficult as they are limited by the information known at the time of prediction and uncertainty in future conditions (Pagano et al., 2004).

To combat this uncertainty, forecasters should perform cross-validation, be wary over-fitting, use novel metrics and search for the optimal combination of predictors (Garen, 1992; Mendoza et al., 2017). Despite these best practices, studies across the western United States have shown that summer runoff has become more variable, even in places that have not experienced recent shifts in climate (He et al., 2016), and that traditional SWE metrics may become less accurate at predicting seasonal droughts (Livneh & Badger, 2020; Vano, 2020). Recent work in snow-dominated watersheds has addressed the declining accuracy of SWE metrics to predict summer runoff by showing the benefit of adding information about antecedent moisture conditions. These antecedent metrics can improve estimates of spring runoff efficiency or how much snow becomes streamflow as opposed to evapotranspiration (ET) (Castillo et al., 2003; Hammond et al., 2019; Lapides et al., 2022). Specifically, it has been recommended to use mean January runoff as a regression predictor of annual streamflow as a way to represent antecedent groundwater conditions (Brooks et al., 2021) or to use soil moisture data (Harpold et al., 2017; Koster et al., 2010). However, many areas still do not have a long enough soil moisture period of record to integrate into regression-based models; furthermore, ice cover can affect the accuracy of winter runoff measurements (Melcher & Walker, 1992). With the declining efficacy of traditional SWE metrics, it is vital to understand the processes that drive changes in runoff efficiency in seasonally snow-covered areas and develop mechanistic models and metrics that represent these processes at a timescale useful for seasonal predictions.

1.2 | Uncertainty in changing snow dynamics and runoff efficiency

High-elevation mountainous regions are projected to warm faster than low-elevation areas (Pepin et al., 2015). With warming, much of the western United States may experience a transition from snow to rain (Klos et al., 2014), declining snowpacks (Mote et al., 2018), and earlier and potentially slower snowmelt (Musselman et al., 2017), which could have a profound impact on streamflow, and contribute to the declining ability of April 1st SWE to accurately predict runoff (Barnett et al., 2005; Goulden & Bales, 2014; Livneh & Badger, 2020). With changing melt rates, it is unclear how changes in the timing and rate of snowmelt will affect the amount of melt that goes to ET. Previous work suggests that lower snow accumulation and earlier melt may lead to earlier increases in ET and the start of the growing season (Cooper et al., 2020; Hamlet et al., 2007; Kraft & McNamara, 2022). If this is the case, more snowmelt may go to ET and less to groundwater recharge and annual runoff (Barnhart et al., 2016; Christensen et al., 2021; Goulden & Bales, 2014).

At the same time, other studies have found no change in streamflow with earlier melt (Hammond & Kampf, 2020), suggesting that snowmelt occurring when there is lower evaporative demand offsets the impact of a transition from snow to rain on runoff efficiency (Barnhart et al., 2020; Robles et al., 2021). These opposing results suggest that the hydrologic responses of changes in snow accumulation and melt may be dynamic and vary both regionally and temporally.

Three primary mechanisms have been proposed to explain variable responses of streamflow to changes in snow accumulation and melt (Gordon et al., 2022). The first mechanism considers the magnitude of winter vapour fluxes such as sublimation in reducing how much water enters the ground; the second emphasizes the importance of rain and snowmelt input intensity (referred to here as surface water inputs); and the third is based on snow-energy synchrony, which controls how much snowmelt goes to ET. Another way to consider the third mechanism is to explicitly consider snow-vegetation interactions and the synchrony of vegetation greening or ET with snowmelt.

Previous work in the forested southeastern United States found that longer growing seasons and changing vegetation dynamics are driving nonstationary changes in catchment storage and ET (Hwang et al., 2018). In a global analysis, Knighton et al. (2020) found that the alignment of climate and vegetation phenology determines how streamflow responds to forest disturbance. In snow-dominated regions with seasonal offsets in the timing of water inputs and the growing season, they found a dampened streamflow response to changes in forest cover. This period between snowmelt and vegetation green-up, referred to as the vernal window, plays an important role in modulating spring runoff and dictating how snowmelt is partitioned into ET (Barnett et al., 2005; Grogan et al., 2020; Stewart et al., 2005). Many studies have found that vernal windows are lengthening due to earlier snowmelt outpacing changes in the start of the growing season (Grogan et al., 2020); however, this asymmetrical shift largely depends on the climate and vegetative characteristics of a region. These studies highlight the important role that the timing of snowmelt and green-up play on runoff generation processes; however, there is currently no consensus on how to account for these dynamics in regression-based predictive streamflow models. Most new metrics of antecedent moisture focus on absolute water deficits

as opposed to timing, and very few explicitly account for changing vegetation dynamics.

1.3 | Underrepresentation of forest processes in seasonal forecasts

Forests impact the magnitude and timing of streamflow generation, yet there is a substantial gap in relating forest processes to downstream water supplies, particularly in irrigated areas (Barnard et al., 2023). In seasonally snow-covered areas, forest structure, such as stem density and canopy cover, affects the amount of precipitation that is intercepted and sublimated (Montesi et al., 2004; Sexstone et al., 2018) and the energy balance of the surrounding snowpack (Kraft et al., 2022; Lawler & Link, 2011; Lundquist et al., 2013; Musselman et al., 2012). Forests also stabilize soils and provide clean water, making them crucial for watershed health and function (Bonan, 2008).

As precipitation regimes change and drought becomes more frequent and severe (Dai, 2013), many regions have started experiencing widespread forest disturbance due to drought-induced mortality, beetle die-off and wildfire (Abatzoglou & Williams, 2016; Adams et al., 2012; Seidl et al., 2017). Each of these disturbances may impact runoff efficiency, though the magnitude and direction of this impact will depend on local geology, topography, climate and vegetation successional classes (Goeking & Tarboton, 2020). Even in regions that have yet to experience large-scale disturbances, changes in local climate may exacerbate or alter how forest structure impacts local hydrology. For example, warmer winters and springs may lead to more canopy interception, early snowmelt and a diminished benefit of canopy shading for snow retention (Dickerson-Lange et al., 2021; Lundquist et al., 2013). Additionally, the amount of forest ET depends on atmospheric evaporative demand and each tree's physiological response to increasing water deficits (Martínez-Vilalta & Garcia-Forner, 2017; Massmann et al., 2019), making it difficult to predict how forests with diverse vegetation will respond to drought. The response of vegetation and ET to warmer and drier conditions has been shown to determine how watersheds and streamflow respond to and recover from drought (Avanzi et al., 2020; Maurer et al., 2022), or, in some cases, explain why watersheds experience a hydrologic regime shift following severe drought (Peterson et al., 2021).

The complex interplay of climate and forest structure, and the effects of vegetation–climate interactions on the hydrologic cycle, make it challenging to capture these dynamics in real time, let alone ahead of time, as needed for seasonal predictions. Thus, few seasonal models integrate information about forest dynamics. Those rare exceptions often use a relatively static metric of percent forest cover, which fails to capture intra-annual changes in vegetation dynamics (Hernandez et al., 2018; Sun et al., 2014).

Here, we address this knowledge gap by introducing a new metric, the Vegetation-Water Alignment Index (VWA), to investigate whether a metric that leverages dynamic vegetation behaviour can improve runoff predictions following a multi-year drought. The VWA quantifies the alignment between vegetation greenness and water availability, thereby both capturing changes in forest structure and providing an inference into water-energy synchrony. Summer runoff and low flows can retain a memory of the previous year's snowpack and storage deficits (Brooks et al., 2021; Godsey et al., 2014; Lapides et al., 2022). Therefore, we hypothesize that when annual snowmelt and rain inputs are more aligned with seasonal vegetation greenness, less snowmelt will go to runoff and recharge, which will reduce the following spring's runoff efficiency. Using a case study from the Greater Yellowstone Ecosystem, we select and validate new predictive models and show how including metrics of evaporative demand and vegetation dynamics improve seasonal predictions of summer runoff. These results emphasize the importance of explicitly accounting for vegetation dynamics as the mechanisms and relationships used to predict streamflow change with droughts and declining snowpacks.

2 | METHODS AND SITE

2.1 | Study site

The Henrys Fork of the Snake River (hereafter referred to as the Henrys Fork) is a major headwater tributary of the Snake River in eastern Idaho, USA (Figure 1b,c). The Henrys Fork is located in the Greater Yellowstone Ecosystem and sourced by three subwatersheds (from here on referred to as watersheds)—the Upper Henrys Fork, Fall River and Teton River—that collectively supply ~25% of the water supply in the upper Snake River basin and the nearly $10 billion agricultural economy that exists in the basin (Idaho Water Resource Board, 2009; Van Kirk et al., 2019). Like many river basins across the western United States, the Henrys Fork is a seasonally snow-covered, forested headwater system that supplies water to downstream users and is expected to see shifts in climate and runoff reliability (Hostetler et al., 2021). As such, this region serves as a case study to investigate the effects of changing vegetation, snow and energy alignment on seasonal runoff predictions and runoff efficiency.

The hydrology of both the upper Snake River basin and the Henrys Fork reflects the complex volcanic geology of the region that formed in the wake of the migration of the Yellowstone Hotspot (Pierce et al., 2007). Due to the unique combination of geology, topography and hydrology, each watershed exhibits distinct streamflow generation processes. As seen in Figure 1a, the Upper Henrys Fork (HF) has the greatest groundwater contribution with higher winter runoff, lower and earlier spring runoff and higher summer baseflows. A majority of the groundwater that feeds the Upper Henrys Fork discharges from a series of springs that emerge at the foot of the Yellowstone Plateau, a nearly 400-m thick rhyolite tuff from the recent Lava Creek eruption (~600 Ka; Pierce & Morgan, 1992). Snowmelt on the plateau recharges the springs' aquifer, which has a response time of approximately 3 years (Benjamin, 2000). The spring discharge joins the rest of the Upper Henrys Fork, which flows through a legacy caldera before descending onto the Eastern Snake

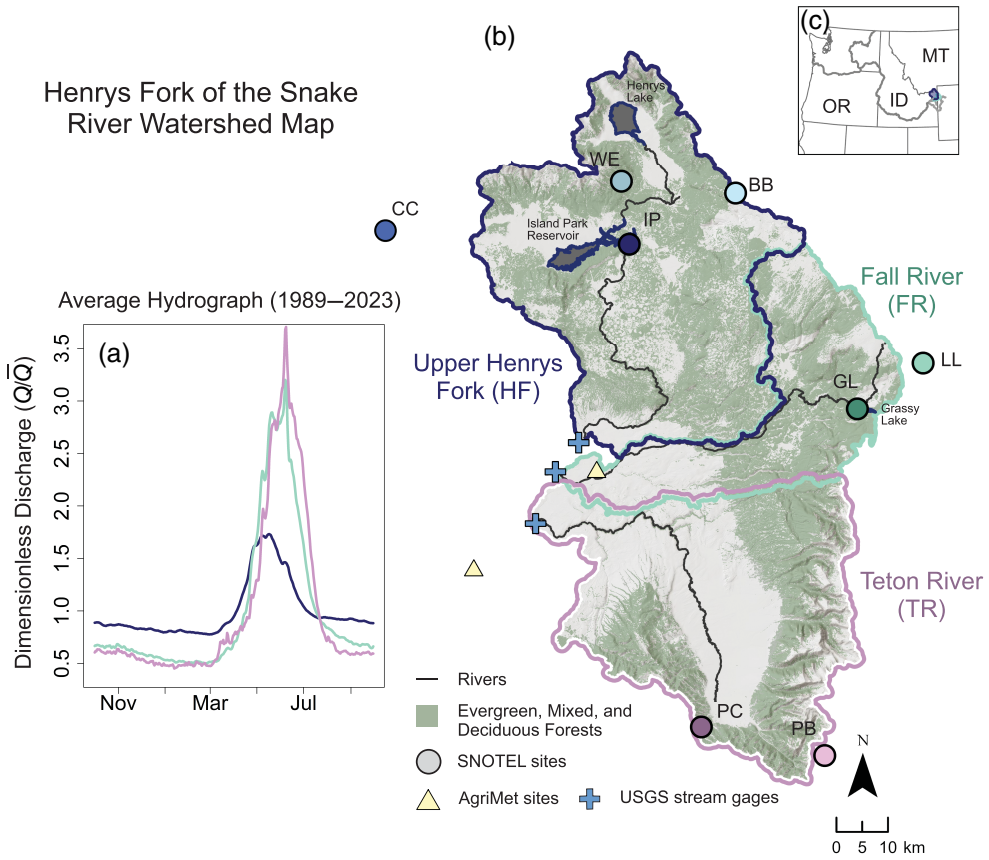

FIGURE 1 Overview of the headwater tributaries of Henrys Fork of the Snake River. (a) Dimensionless discharge (average daily streamflow/annual average daily streamflow) using 1989–2023 averages to show the distribution of flow throughout the water year (October–September) and highlight the distinct runoff generation processes in each watershed. The colour of each line represents the corresponding watershed, as labelled on the site map. (b) Watershed map of the three focal subwatersheds, the Upper Henrys Fork (HF), Fall River (FR) and Teton (TR), with the location and site codes of NRCS SNOTEL sites, USGS stream gages and Reclamation AgriMet sites used in this study. Table S1 gives description of each SNOTEL site. Green shading indicates land classified as evergreen, mixed or deciduous forests Dewitz, (2023). The colour of each SNOTEL site indicates the watershed that site is associated with and the shading indicates the relative elevation of the site where a darker colour indicates a lower elevation. (c) Regional site map of the Henrys Fork, a major headwater tributary in the Columbia-Snake basin.

River Plain. The Upper Henrys Fork has the lowest average elevation, followed by Fall River and Teton River, as seen in Figure S1.

In contrast to the strong groundwater influence in the Upper Henrys, Teton River is strongly snowmelt-dominated, with most of the water supply coming from snow that falls in the Teton Range. Figure 1a shows the high spring flows and lower summer baseflows indicative of snowmelt-driven runoff. The remaining watershed, Fall River, is sourced by a mix of groundwater springs and snowmelt, resulting in a more intermediate hydrograph shape (Figure 1a).

The climate of the study area transitions from warm continental at low elevations to dry-summer subarctic at high elevations (Kottek et al., 2006). Across all three watersheds, there is a sharp precipitation gradient with around 300 mm of annual precipitation in the valleys and up to 2000 mm in the high-elevation mountains, with anywhere from 50% to 80% falling as snow, depending on elevation. The Greater Yellowstone Climate Assessment projects that this region will receive more annual precipitation, but a lower snow fraction, in the coming decades (Hostetler et al., 2021).

A large portion of each watershed is forested, as seen with the green shading in Figure 1b. The composition of these forests varies by elevation and aspect but are largely dominated by lodgepole pine (*Pinus contorta*), Engelmann spruce (*Picea engelmannii*), Douglas-fir (*Pseudotsuga menziesii*), whitebark pine (*Pinus albicaulis*) and subalpine fir (*Abies lasiocarpa*). These forests experienced substantial disturbance before the 1989 start of this study due to a combination of extensive timber harvesting and the 1988 Yellowstone Fires (Turner et al., 2003). Though most of the fire perimeter was outside of the watershed, with less than 5% of both the Upper Henrys and Fall River watersheds affected (Figure S2), beetle infestation following the fires led to additional delayed mortality in the early 1990s (Ryan & Amman, 1996). While there has been a recent resurgence of beetle mortality in the eastern Greater Yellowstone Ecosystem, the Henrys

Fork has experienced only small-scale disturbances in the past 20 years.

2.2 | Data

2.2.1 | Natural streamflow data

Water resources in the Henrys Fork are highly regulated by irrigation storage, delivery and return flow (Morrisett et al., 2023). In this study, we use natural streamflow (Q_{nat}) to refer to unregulated runoff in each watershed (Van Kirk, 2020), calculated as:

$$Q_{nat} = Q_{reg} + \text{diversions} + \Delta S + E_{res} - \text{injection} \quad (1)$$

where Q_{reg} is regulated streamflow at the USGS gage, diversions are surface water diversions recorded daily by Idaho Water District 01, ΔS is change in upstream reservoir storage, E_{res} is upstream reservoir evaporation and injection is input to streamflow upstream of the gage via delivery of water from other watersheds through canals or via exchange wells, which pump groundwater directly into rivers (U.S. Bureau of Reclamation and Idaho Water Resource Board, 2015). Direct precipitation onto the reservoir is included in the reservoir evaporation term, making E_{res} negative when precipitation exceeds evaporation. As each watershed has different infrastructure, the application of Equation (1) varies slightly between each watershed. A full description of these differences can be found in Supporting Information Text S1. The normalized discharge shown in Figure 1a is the mean daily natural streamflow on any given day of the year divided by the 1989–2023 annual average daily natural streamflow.

2.2.2 | SNOTEL data

The precipitation, SWE and snow depth data used in this study come from all of the Natural Resources Conservation (NRCS) Snow Telemetry (SNOTEL) sites in and near the study watersheds (Figure 1b). Key topographic and vegetative characteristics of each site are given in Table S1. As advised by NRCS, the temperature data were corrected to resolve a known bias associated with a change in sensor (Atwood et al., 2023). Since hourly instantaneous data was not available for the entire period of record for all sites, we applied the correction equation to daily summary statistics. Over the relevant range of temperatures for a given day, the correction is nearly linear, indicating that applying the correction directly to the daily mean summary statistic is close to the true mean. We performed the analyses outlined below with both the daily mean and the mid-point of the range in daily minimum and maximum temperatures. We found no difference, and therefore, present the results using mean daily temperatures.

Using the SNOTEL SWE data, we calculated daily melt rates as the decrease in SWE. We also partitioned daily precipitation into rain and snow by classifying days with precipitation and an increase in snow depth or SWE as 'snowy' and days with new precipitation but no change or a decrease in snow depth or SWE as 'rainy' (Jennings & Molotch, 2019). Using this melt and rain data, we calculated daily surface water inputs (SWI) as melt plus rain to represent when liquid water enters the system (Kormos et al., 2014).

To compare sites, we will use the term 'lower' to refer to the SNOTEL stations that have an elevation between 1900 and 2100 m, 'mid' to refer to those between 2100 and 2300 m and 'high' to refer to the stations with an elevation greater than 2300 m.

2.2.3 | MODIS NDVI data

The normalized difference vegetation index (NDVI) is a metric of vegetation greenness commonly used to describe growing season dynamics (White et al., 2009), leaf area index (Tewari et al., 2012), forest density and disturbance (Jin & Sader, 2005), and in some areas, NDVI has been shown to have a strong relationship with ET (Goulden et al., 2012). As a broad measure of vegetation dynamics, we use the 250-m MODIS (Moderate Resolution Imaging Spectroradiometer) 16-day NDVI data products from both the Terra and Aqua satellites (MOD13Q1 and MYD13Q1, collectively referenced as M*D13Q1). Together, these products produce a 20-year time series that are widely used and publicly accessible through open-source software. Before release, the 16-day NDVI products are internally processed for atmospheric correction and cloud cover, with the highest quality image and highest NDVI value selected for each pixel with the corresponding day of acquisition recorded (Didan et al., 2015). To further process this data, we used the M*D13Q1 reliability index to filter out any remaining low-quality pixels associated with cloud cover or interference other than snow cover. After filtering out low-quality pixels, we used the NDVI and the day of image acquisition for each pixel to generate a time series of average watershed NDVI, average watershed annual maximum NDVI and time series of NDVI extracted at the pixel containing each SNOTEL site location.

As a spectral index, NDVI is affected by snow cover extent (Wang et al., 2013), suggesting that in seasonally snow-covered areas, winter NDVI values will represent both vegetation greenness and snow cover. To retain an annual time series and incorporate insight associated with snow-covered extent and frequency (Hall & Riggs, 2007), we deliberately retained values flagged as snow-covered if the image was otherwise high quality. Once processed as described above, NDVI values show some variability related to early winter snow accumulation and depth, but are fairly consistent during mid-winter months (Figure S3).

2.3 | Time trend analysis

To investigate whether predictors of summer runoff in this region have changed, we used modified time trend analysis. Time trend analysis can be used to isolate the impacts of changes in climate or vegetation on streamflow, such as the effects of forest disturbance on watershed yield (Goeking & Tarboton, 2022; Manning et al., 2022;

Zhao et al., 2010). This is done by fitting a regression model to a pre-disturbance calibration period and testing whether the difference between the observed and predicted values for the post-disturbance period is significantly non-zero. If they are non-zero, this implies that the predictive relationships have changed between the calibration and test periods. For example, this method might use annual precipitation and temperature to predict annual runoff before and after a disturbance. Here, we use a modified approach to quantitatively investigate whether the relationships used to predict summer streamflow during and after drought differ from pre-drought relationships. In this modified approach, we use seasonal predictive models of summer runoff and test whether a multi-year drought changes runoff predictability. To delineate pre-drought, drought and post-drought periods, we performed linear breakpoint analysis on a time series of the Palmer Drought Severity Index (PDSI) averaged across all three watersheds (accessed via ClimateEngine.org; Huntington et al., 2017). We used the resulting breakpoints to define pre-drought, drought and post-drought periods and investigate non-stationarity in predictive relationships as detailed below.

For the pre-drought predictive model, we use April 1st SWE and mean January runoff to predict summer runoff for each watershed, as given in Equation (2) where log represents the base-e logarithm.

$$\log(\text{summer runoff}) = \beta_0 + \beta_1 \log(\text{April 1 SWE}) + \beta_2 \log(\text{Jan. runoff}) \quad (2)$$

Here, runoff refers to area-normalized Q_{nat} (mm). Summer runoff is total runoff from April 1st–September 30th and Jan. runoff is mean daily January runoff (mm). April 1st SWE is the average from all SNOTEL sites in or near each watershed (Figure 1b). We define summer runoff as runoff between April and September due to peak irrigation demand in the region occurring in July and August: this acknowledges the importance of predicting runoff through the irrigation season (past the commonly used April–July timeline). We include January runoff as it has been demonstrated to represent antecedent groundwater conditions and improve streamflow predictions in snow-dominated watersheds (Brooks et al., 2021). Although other factors inevitably influence summer runoff, we emphasize that this is a seasonal predictive model, and therefore, we can only include variables known by April 1st, when seasonal predictions are made. We used the pre-drought water years of 1989–1998 to calibrate the models using Equation (2). The Teton River model has a slight modification where we used April 1 SWE without a log transformation to improve the normality and leverage of the residuals. The normality of the residuals was confirmed with a Lilliefors test (Lilliefors, 1967) and the homoscedasticity of the residuals with scatterplots of residuals versus summer runoff and water year.

We then applied the pre-drought model to the drought and post-drought periods and calculated ΔQ_{nat} as observed natural runoff—predicted natural runoff, so ΔQ_{nat} is negative when the model over-predicts runoff. We used a one-sample *t*-test to test whether ΔQ_{nat} for the water years in each period is non-zero. If ΔQ_{nat} is non-zero, this suggests the accuracy of summer runoff predictions has changed due to something other than April 1st SWE and antecedent groundwater. To facilitate comparison of ΔQ_{nat} across watersheds, we calculated the percent deviation of observed from predicted runoff using Equation (3).

$$\text{Percent Deviation}\,(\%) = \frac{(\text{Observed} - \text{Predicted})}{\text{Predicted}} \times 100 \quad (3)$$

2.4 | Climate and vegetation analysis

Next, we investigated changes in climate and vegetation that may impact runoff efficiency. To do this, we ran Mann–Kendall trend analysis on a variety of temperature, precipitation and vegetation metrics. The nonparametric Mann–Kendall trend test detects monotonic increasing or decreasing trends over time (Helsel et al., 2020). In this study, we performed this analysis over the entire period of record (1989–2023) to detect long-term trends in each watershed. For our climate analysis, we analysed average annual, winter, early spring, late spring, summer and fall temperatures. To detect changes in precipitation and snow accumulation, we analysed total annual precipitation, peak SWE, snow fraction (peak SWE/annual precipitation) and the day of peak SWE. Each precipitation metric represents the average of the SNOTEL site data in or near each watershed (Figure 1b).

Similarly, to detect changes in vegetation, we performed Mann–Kendall trend analysis on watershed-averaged maximum NDVI ($NDVI_{MAX}$) and fractional tree cover. Given the changes in data availability and satellite platforms since 1989, we calculated trends for $NDVI_{MAX}$ for 1989–2012 using the 1-km resolution Advanced Very-High-Resolution Radiometer (AVHRR) and for 2001–2023 using 250 m MODIS NDVI data separately. We chose to do this to limit uncertainty associated with spatial and temporal resampling techniques (Huang et al., 2021; van Leeuwen et al., 2006). If both the AVHRR and MODIS trends are significant, we can assume that $NDVI_{MAX}$ has changed over the period of record. As a second measure of vegetation dynamics, we used the 30 m resolution National Land Cover Database's RCMAP fractional tree cover data to calculate watershed-averaged percent tree cover (Rigge et al., 2021). The fractional data give the proportion of tree canopy per pixel, so a change in watershed-averaged cover may represent a change in the number of pixels with tree cover (forest extent) or the percent tree cover in each pixel (forest density). The time series of fractional tree cover is highly auto-correlated, so we performed a modified Mann–Kendall that accounts for the effective sample size. Mann–Kendall analyses were performed using the Kendall (McLeod, 2022) and modifiedmk (Patakamuri & O'Brien, 2021) R packages.

2.5 | Vegetation-water alignment

To test whether adding information about vegetation dynamics improves runoff predictions, we introduce a metric that captures changes in both vegetation and water availability, or the water-

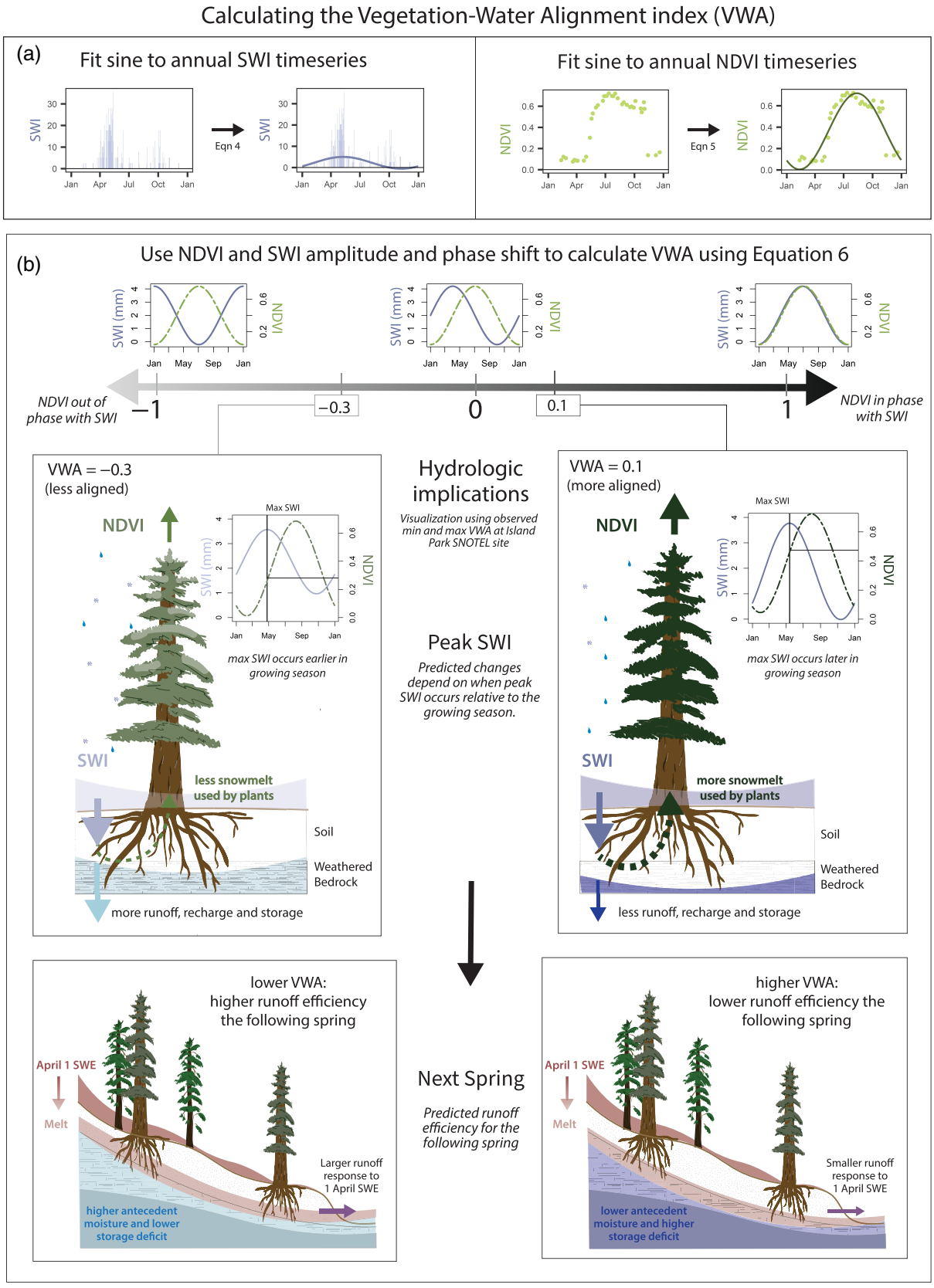

FIGURE 2 Conceptual diagram providing a visual description of (a) vegetation-water alignment index (VWA) calculations fitting sine curves to annual surface water inputs (SWI) and normalized difference vegetation index (NDVI) data. (b) Conceptual hypothesis proposing how different values of VWA and associated SWI-NDVI synchrony affect recharge, antecedent conditions and subsequent runoff efficiency.

growing season alignment. To characterize alignment, we use a similarity index that quantifies how in-phase calendar year NDVI is with SWI, which we will refer to as the VWA. As described in Section 2.2.2, SWI is the combination of snowmelt and rain, which represents when liquid water enters the ground. As with previous studies that calculate similarity indices using different climatic variables (Apurv & Cai, 2020; Hale et al., 2023; Woods, 2009), we first fit a sine curve to calendar year SWI at each SNOTEL site (Equation 4). For the purpose of capturing key characteristics of the seasonal periods, we assume that a single sine curve can reasonably fit SWI data, an assumption often used for precipitation, temperature and ET data, particularly in snow-covered regions (Apurv & Cai, 2020; Berghuijs & Woods, 2016; Hale et al., 2023; Milly, 1994; Potter et al., 2005; Woods, 2009). Figure 2a graphically summarizes Equations (4–6) and their interpretation.

$$\mathrm{SWI}(t) = \overline{\mathrm{SWI}}\left[1 + \delta_{\mathrm{SWI}} \sin\left(\frac{2\pi(t - s_{\mathrm{SWI}})}{365}\right)\right] \quad (4)$$

In Equation (4), $\overline{\mathrm{SWI}}$ is mean annual SWI, δ_{SWI} is the dimensionless amplitude, t is time in days and s_{SWI} is the phase shift in days. Text S2 in the Supporting Information provides an overview of using a sine function in this context and a discussion of Equations (4 and 5) within the context of the general sine form.

To integrate the annual variability of vegetation dynamics into this metric, we also fit a sine curve to calendar year MODIS NDVI extracted to each SNOTEL site (Equation 5), where δ_{NDVI} is the dimensionless amplitude of the sine curve and s_{NDVI} is the phase shift in days.

$$\mathrm{NDVI}(t) = \frac{1}{2}\mathrm{NDVI}_{\mathrm{MAX}}\left[1 + \delta_{\mathrm{NDVI}} \sin\left(\frac{2\pi(t - s_{\mathrm{NDVI}})}{365}\right)\right] \quad (5)$$

Here, we account for interannual variability in NDVI by multiplying by half of $\mathrm{NDVI}_{\mathrm{MAX}}$ instead of mean annual NDVI. Previous work has shown that maximum NDVI is a more reliable way of compositing NDVI given the heavy influence of cloud and atmospheric contamination on mean NDVI (Holben, 1986; Zhang et al., 2017). Fitting an annual sine curve requires year-round values of NDVI, further supporting the retention of winter NDVI values as described in Section 2.2.3. Since the mid-winter values show low variability, winter NDVI sets the bottom of the annual cycle: changes in phase and amplitude primarily reflect the timing of snow disappearance and peak greenness. For both SWI and NDVI, sine functions were fit to annual data using the iterative, non-linear least-squares function 'nlsLM' in the R package minpack.lm (Elzhov et al., 2023). Figure 2a shows an example of how sine curves fit annual cycles of SWI and NDVI.

The phase and amplitude of each annual curve can be related using a similarity index, as given with Equation (6), which is weighted by the amplitude of NDVI and quantifies whether NDVI is in phase with SWI (Berghuijs et al., 2014; Woods, 2009). The VWA, or the similarity index of SWI and NDVI, ranges from close to −1 to 1, depending on δ_{NDVI}. A value closer to −1 indicates that NDVI is out-of-phase with SWI and +1 that NDVI and SWI are in-phase.

$$\mathrm{VWA} = \delta_{\mathrm{NDVI}}\,\mathrm{sgn}(\delta_{\mathrm{SWI}})\cos\left(\frac{2\pi(s_{\mathrm{NDVI}} - s_{\mathrm{SWI}})}{365}\right) \quad (6)$$

Here, sgn refers to the sign (positive or negative) of δ_{SWI}, which is used to assess whether NDVI and SWI periods exhibit the same seasonality (i.e., if the peaks both fall in the first or second 6 months of the year or not). To capture dynamic changes in vegetation, Equation (6) scales the distance of the phase shifts by δ_{NDVI}. This is done so that when there is little annual variability in NDVI (a δ_{NDVI} closer to 0), VWA will also be closer to 0. When NDVI shows strong annual variability, and therefore, has a higher δ_{NDVI}, this scaling will move the value closer to ±1, with the sign dependent on the difference in phase shifts. Given the seasonal snow cover and energy limitations on the growing season, we do not observe the full range of possible VWA values in this system. Figure 2b gives an example using the NDVI and SWI curves associated with the lowest and highest observed VWA at the Island Park (IP) SNOTEL site. This example demonstrates how a shift in VWA can reflect changes in timing of peak SWI and greenness as well as the amplitude of NDVI. For a conceptual overview of the components of SWI and NDVI sines curves and a visualization of how shifts in each variable's amplitude and phase shift affects VWA, see Figures S4 and S5.

Using Equations (4–6), we calculated VWA for each SNOTEL site in or near the watershed boundaries, except for Crab Creek (CC). We use the CC SNOTEL site for Upper Henrys meteorologic averages, but did not calculate VWA for that station as it did not have snow depth data available for the entire record.

We propose using VWA as a metric that integrates information about water-growing season alignment, changes in peak NDVI and changes in the annual distribution of SWI, all of which may influence annual runoff efficiency in seasonally snow-covered watersheds (Gordon et al., 2022). Given the memory that many watersheds have of antecedent moisture conditions (Brooks et al., 2021; Castillo et al., 2003), we propose that the alignment of NDVI with SWI for a given calendar year can be used to represent the relative storage state of the catchment at the end of the year and therefore be used to scale the following spring's seasonal runoff predictions. Figure 2b shows our hypothesis that when NDVI and SWI are more aligned, less melt and rain will go towards runoff and recharge. Instead, when peak SWI is more closely aligned with the start of the growing season, more of the snow meltwater entering the soil will be taken up by plants and lost to ET, creating a storage deficit. This is visualized in Figure 2b using arrow size to represent the relative flux of SWI, plant water uptake and runoff and recharge. Following a closely aligned year, we hypothesize that the memory of this reduced recharge will be carried over through a storage deficit that leads to lower runoff efficiency for a given snowpack the following spring. We propose that this lower runoff efficiency is due to the storage deficit needing to be refilled before runoff is produced (McDonnell et al., 2021).

2.6 | New predictive model selection and validation

2.6.1 | Model selection

To investigate whether VWA, or some other new metric, adds predictive power compared with traditional snowmelt-based models of streamflow (e.g., Equation 2) in the post-drought period, we performed statistical model selection using Akaike's information criterion (AIC) to rank models and select a new predictive model for the post-drought period in each watershed. We created models for the post-drought period to ensure consistent periods of record for all satellite and sensor data and to ensure the model is trained with years with similar forest cover and vegetative state. Here, we refer to the selected regression models as the 'new' models and the predictive models fit with April 1 SWE and January runoff (Equation 2) as the 'traditional' models.

To select the best new models for each site, we provided a set of candidate predictor variables to generate potential models and then ranked them according to AIC, which measures the variation explained by each model and the complexity of the model relative to the other candidate models (Claeskens & Hjort, 2008). All candidate predictors are listed and defined in Table S2. Given the short post-drought period of record, we used the small-sample-corrected AIC, referred to as AICc. Model selection was performed using the MuMIn: Multi-Model Inference package in R version 4.2.3 (Bartoń, 2023).

2.6.2 | Cross validation

After model selection, we performed leave-one-out cross-validation to test the predictive performance and bias of the new models. To do this, we iterated through each predicted year of the post-drought period (2007–2023), fit a model using all but the selected year, and then used that model to predict runoff for the year not included in the model fit. To assess model performance, we calculated Nash–Sutcliffe efficiency (NSE), model percent bias (PBIAS) and root mean square error (RMSE) using the observed and predicted values. To facilitate comparison across watersheds, we scaled RMSE by the standard deviation of observed summer runoff, referred to here as $RMSE_{sd}$ (Moriasi et al., 2007). To compare the improvement offered by these new models, we also performed cross-validation on the traditional model using April 1 SWE and January runoff. By comparing performance metrics between the models, we can quantify the predictive improvement offered by the new model over the traditional one.

3 | RESULTS

3.1 | Time trend analysis

3.1.1 | Post-drought over-prediction

Breakpoint analysis of PDSI revealed three breakpoints delineating the pre-drought period as water years (October 1–September 30) 1989–1998, the drought period (including drought development and recovery) as 1999–2005 and post-drought as 2006-present, as shown in Figure 3a by the solid lines. Applying the pre-drought models to the drought period, we see the model significantly over-predicted runoff in Fall River and Teton River ($p < 0.05$), but differences between measured and modelled runoff were insignificant in the Upper Henrys. Metrics of the pre-drought traditional model fits are given in Table S3. Figure 3c,d shows that the time series of percent deviation of observed from expected runoff is below zero in these two watersheds for most of the drought period, meaning that observed runoff was consistently lower than expected in the drought period. Figure 3e shows the average ΔQ_{nat} for each watershed, with significance noted for periods when ΔQ_{nat} was significantly non-zero.

The average ΔQ_{nat} improved from the drought to post-drought period in Fall and Teton Rivers. While the model over-predicted post-drought runoff, the over-predictions were insignificant. In the Upper Henrys, we see significant over-predictions and declining post-drought model performance ($p < 0.1$). The observed over-prediction in the drought and post-drought periods suggests that the system has experienced mechanistic changes affecting runoff efficiency not captured by the pre-drought relationships between April 1 SWE, January runoff and summer runoff.

3.1.2 | Changes in climate and vegetation

To investigate other potential drivers affecting the reliability of the historic stream-snowpack relationship, Figure 4 summarizes results from Mann–Kendall trend analyses on temperature, precipitation and vegetation metrics in each watershed for the 1989–2023 record. All metrics represent the average of the SNOTEL sites in or near each watershed (Figure 1b). The top set of metrics includes average annual and seasonal temperatures for winter (December, January, and February), early spring (March and April), late spring (May and June), summer (July, August, and September) and fall (October and November). Each box is coloured by the Kendall's tau of the trend where green indicates an increasing trend and brown indicates decreasing. Significant trends are labelled with asterisks. This trend analysis reveals that late springs and summers are now significantly warmer in the Upper Henrys Fork and Teton River watersheds than at the start of the study period. The Teton River watershed is the only watershed that has seen significant annual warming. Comparison of precipitation metrics, including water year total annual precipitation, day of peak SWE, annual max SWE and snow fraction (peak SWE/annual precipitation), reveal no significant trends in any watershed (Figure 4).

Analysis of vegetation metrics shows that $NDVI_{MAX}$ is significantly increasing over both satellite periods of record in the Upper Henrys Fork. We also see a significant increase over the AVHRR period of record (1989–2012) in Fall River. Trend analysis of the 1989–2020 fractional tree cover record shows significant increases in percent tree cover in all watersheds in all three periods. Both fractional tree cover and $NDVI_{MAX}$ suggest that forest greenness and density have changed over the course of the study period in the Upper Henrys and Fall River watersheds.

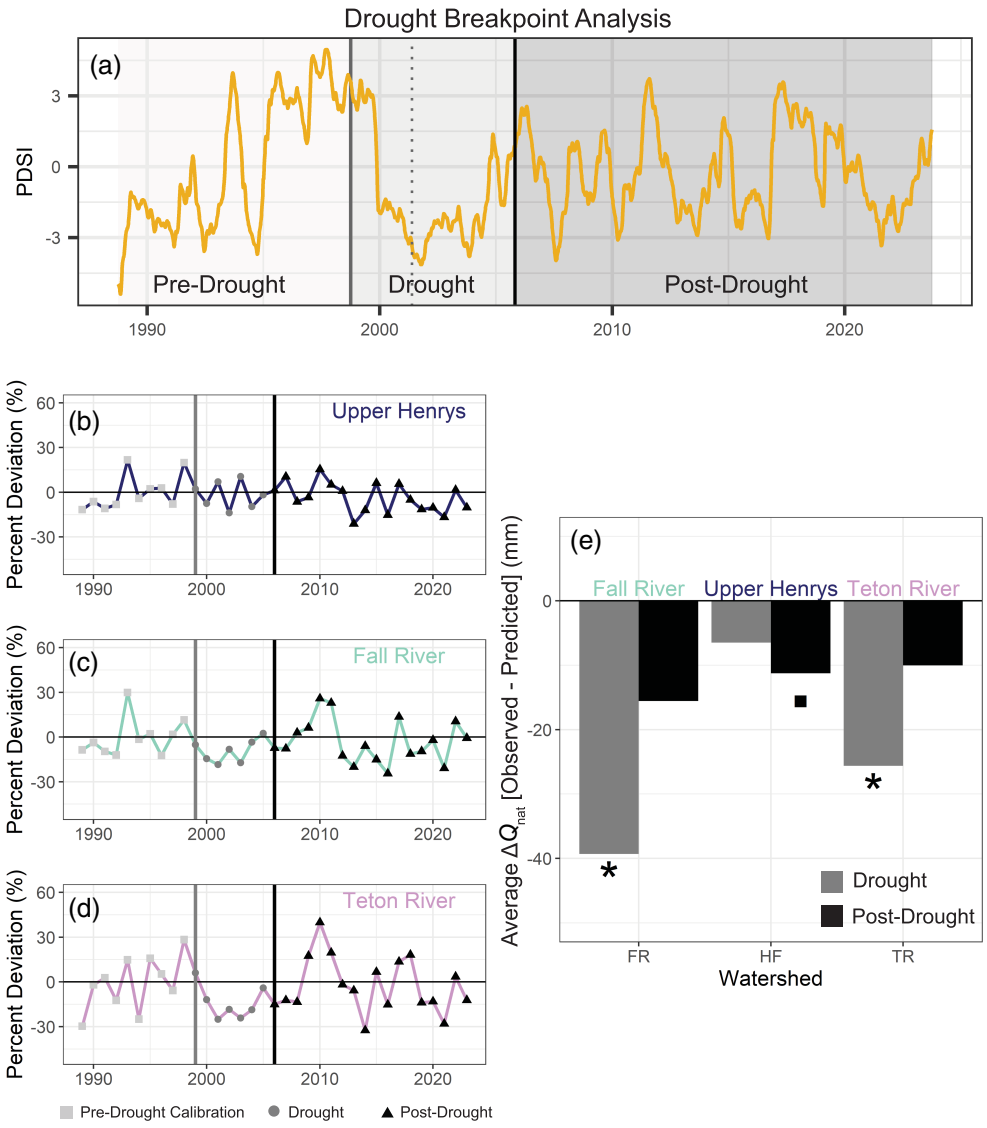

FIGURE 3 (a) Linear breakpoint analysis of spatially averaged Palmer Drought Severity Index (PDSI) for all three watersheds. Breakpoints delineate the 1989–2023 period of record into pre-drought, drought and post-drought periods (solid lines). The dotted line represents the mid-drought breakpoint delineating drought development and recovery. (b–d) Time series of percent deviation of observed from expected runoff using pre-drought calibrated model applied to drought and post-drought periods. Negative percent deviation indicates that the model over-predicted runoff. (e) Bar chart of average ΔQ_{nat} (observed—predicted runoff) for drought and post-drought periods. Significance of one-sample *t*-test test noted by * at $p < 0.05$ and ■ at $p < 0.1$.

3.2 | Vegetation-water alignment index

Figure 5 shows the time series of SNOTEL VWA, with the shade of the line indicating the relative elevation of the site where lower elevation sites are darker and higher elevation sites lighter. To capture the spatial variability of precipitation and greenness across each watershed, we show both a watershed-average VWA using spatially averaged NDVI and the average of all watershed SNOTEL SWI (Figure 5 dashed line). In all watersheds, there is no significant trend since calendar year 2006 in either the SNOTEL point or spatially averaged watershed VWA.

In the Upper Henrys Fork and sometimes in Teton River, the lower elevation SNOTEL point measurements have a lower (more negative) VWA than the higher elevation stations (Figure 5a,c). A more negative VWA signifies that vegetation greenness is more out of alignment with snowmelt and rain entering the system at lower elevations than higher elevations. This may reflect more mid-winter melt events and earlier spring melt due to a lower snow fraction and warmer winter temperatures at lower elevations. This elevational relationship does not occur in Fall River (Figure 5b); however, it is worth noting that the lowest elevation SNOTEL site in Fall River is at the same elevation as the mid-elevation sites in the Upper Henrys Fork (Figure S1).

The dashed watershed-average VWA is often higher than what is captured at the SNOTEL sites, reflecting a closer growing season-water input alignment. However, in each watershed, the spatially averaged VWA is lower than the SNOTEL VWA in 2007 and 2015. Both of these are low snow years where contrasting patterns in the amplitude and phase shift of annual NDVI at the watershed-scale likely reflect early melt and water-limited phenological responses of other vegetation types (shrubs, grasses, crops, etc.) that are present throughout the watershed but not dominant at SNOTEL sites. Underlying all the VWA patterns, we found that annual SWI is far more variable than NDVI, but in many areas, peak NDVI is shifting earlier in the year (Figures S6–S8).

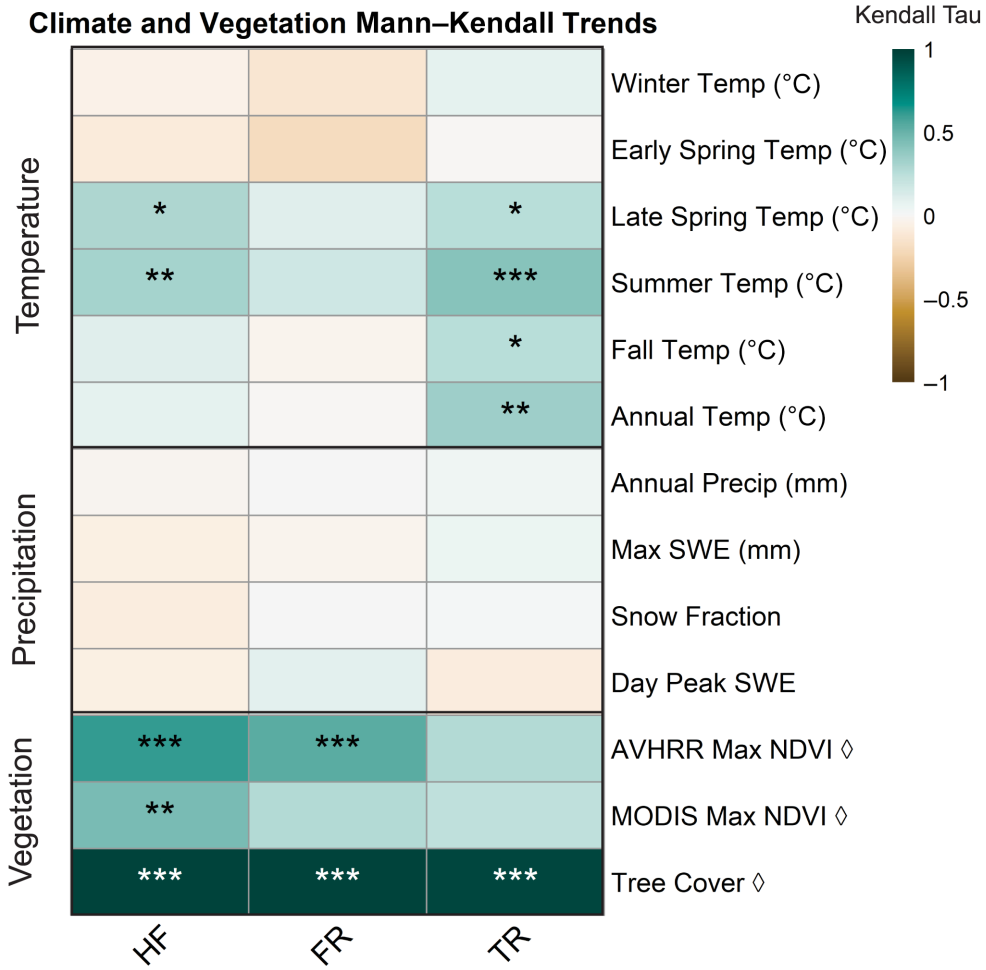

FIGURE 4 Table showing results of Mann–Kendall trend analysis of temperature, precipitation and vegetation metrics for all three watersheds. Each box is coloured by the Kendall tau of the trend where a darker green indicates a stronger increasing trend, and brown, decreasing. Black boxes group the metrics categorically. Significant trends are labelled with *** at $p < 0.001$, ** at $p < 0.01$, * at $p < 0.05$ and variables with periods of record shorter than the 1989–2023 periods of record are indicated with a diamond (◊). Advanced very-high-resolution radiometer (AVHRR) and MODIS refer to the corresponding satellite for each normalized difference vegetation index (NDVI) dataset.

3.3 | Selecting and testing new predictive models

Post-drought AICc model selection shows that VWA is an important predictor of summer runoff. In Teton River and the Upper Henrys Fork, we selected the model with the lowest AICc, both with four fitted parameters. In Fall River, the top three models had similar AICc and we chose the most parsimonious, with only four parameters. Figure 6 shows the new predictive models selected for each watershed and the *z*-score standardized estimates of the coefficient of each predictor. Positive predictors are shown in dark blue and negative in light red. Across all three watersheds, April 1 SWE is the strongest predictor of summer runoff. We also see that the best new model for each watershed includes the previous summer (July–September) average alfalfa reference ET (ETr) from the average of the two valley AgriMet stations (Figure 1b) and a SNOTEL VWA. The same ETr is used for all three watersheds and represents low-elevation evaporative demand. Selected models for each watershed are listed in Tables S4–S6.

Across all three watersheds, VWA is a negative predictor of the following year's summer runoff, meaning the more aligned NDVI and SWI are for a given year, the lower the following year's streamflow response will be for a given snowpack. This supports the conceptual hypothesis presented in Figure 2b. In the Upper Henrys Fork, the low-elevation IP SNOTEL site was selected in the best model. Because Fall River does not have a low-elevation SNOTEL site, we included IP as a potential predictor, which was also selected in the best new model. Additionally, the best model in Teton River included the lowest-elevation Pine Creek station VWA. The best models in each watershed include the same three predictors, revealing the widespread importance of water-climate-growing season interactions and their persistent impact on runoff efficiency.

To test the predictive performance of these models, we report results from leave-one-out cross-validation using the 2007–2023 period of record (Figure 7), highlighting predicted versus observed runoff for each year using the new and traditional predictive models. To facilitate comparison across watersheds, we scaled RMSE by the standard deviation of observed summer runoff, referred to here as $RMSE_{sd}$. An $RMSE_{sd}$ of less than 0.5 indicates good model performance (Moriasi et al., 2007). The summary metrics are given in Table 1.

Overall, we see the best improvement and model performance for each year in the post-drought period in the Upper Henrys with an NSE of 0.79. We also see improvement in Fall River, with an NSE of 0.70 for the new model compared with 0.56 for the traditional model. Teton River shows moderate improvements and performance with an NSE increase from 0.43 to 0.6. In all watersheds, we see low model

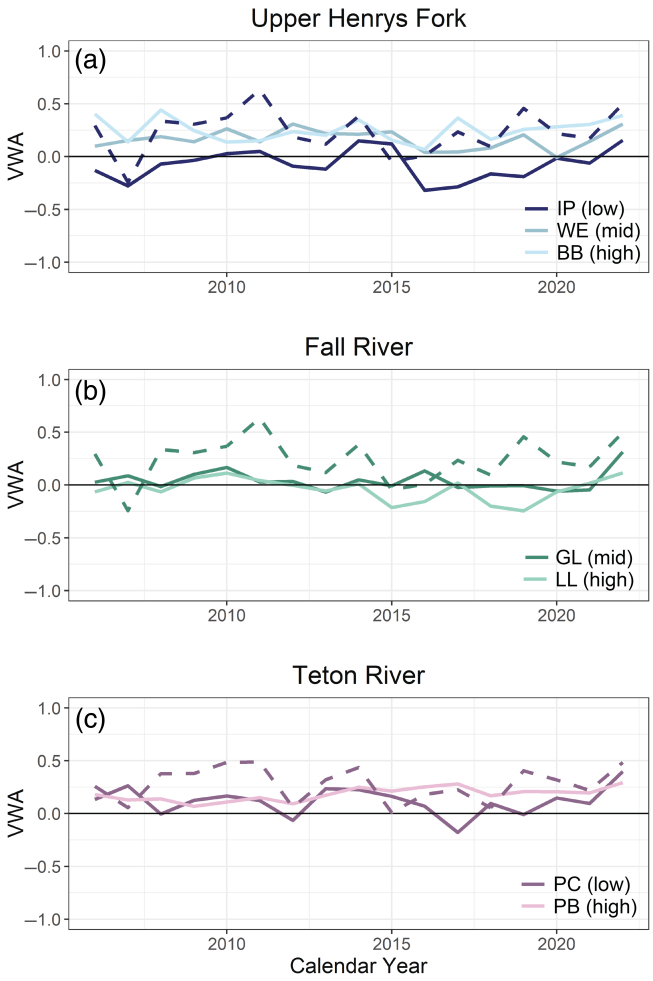

FIGURE 5 (a–c) Time series of SNOTEL and watershed-averaged vegetation-water alignment index (VWA). Dashed lines are the watershed VWA calculated using watershed-average normalized difference vegetation index (NDVI) and SWI averaged across all SNOTEL sites within each watershed. Solid lines are VWA calculated for each SNOTEL station using MODIS NDVI extracted for the station location and SWI site data. Shade of the solid lines indicate the relative elevation of that SNOTEL site compared with other sites within the watershed where a darker shade indicates a lower elevation site. See Table S1 for the site elevations.

biases with slight model under-prediction with the new models. Finally, we see improvements in $RMSE_{sd}$ in Fall River and the Upper Henrys Fork, dropping $RMSE_{sd}$ for both sites close to or under 0.5.

4 | DISCUSSION

4.1 | Non-stationarity of predictive relationships, climate and vegetation dynamics requires new models

In this study, we investigated whether historic relationships between April 1 SWE, winter runoff and summer streamflow still accurately predict summer runoff following the early 2000s severe drought. We analysed model performance before, during and after drought since it is well documented that drought reduces runoff efficiency and decreases the accuracy of seasonal predictive models (Saft et al., 2015; Tian et al., 2018). Furthermore, recent work looking at recovery following Australia's Millennium Drought suggests that some watersheds shift to a new state following severe drought, and that drought recovery is not just linked to catchment wetness, but also changes in vegetation that cause more precipitation to go to transpiration (Peterson et al., 2021).

Time trend analysis results show that the pre-drought relationships over-predict summer runoff during the drought (FR and TR) and post-drought (HF) periods. Before and after the drought, this region has not experienced any widespread changes in annual precipitation, snow accumulation or timing of melt (Figure 4), suggesting that the worsening performance in the Upper Henrys Fork is not due to changes in water inputs. What has changed is warmer late spring and summer temperatures (May through September) in the Upper Henrys Fork and Teton River watersheds as well as vegetation greenness and fractional tree cover. The latter two vegetation metrics increased the most in the Upper Henrys Fork and to lesser degrees in Fall River and Teton River (Figure 4). Our analysis shows that these changes in temperature and vegetation dynamics impact runoff efficiency as all three new models selected for the post-drought period include a metric of the previous summer's evaporative demand (ETr) and vegetation dynamics (VWA).

Collectively, these results affirm that accounting for changing snow dynamics alone may fail to capture important mechanisms underlying changes in runoff efficiency and the relationships used to predict streamflow. These findings also suggest that our understanding of future runoff dynamics hinges on our understanding of climate–vegetation interactions.

4.2 | VWA improves predictions and provides mechanistic insights

The VWA proposed here is a metric that integrates information about changes in annual SWI, snow fraction, snowmelt rate, seasonality of precipitation, snow cover, timing of vegetation green-up, peak greenness, length of growing season and the synchrony of SWI and NDVI. Many of these elements are predicted to change with warmer temperatures and a snow-to-rain transition (Cayan et al., 2001; Klos et al., 2014) and may impact runoff efficiency across multiple timescales (Barnett et al., 2005). Each new model includes a SNOTEL VWA as a negative predictor of summer runoff, with VWA showing up in nearly all the top-ranked models (Figure 6 and Tables S4–S6). The importance of VWA as a negative predictor supports our hypothesis that the more closely aligned NDVI and SWI are for a given calendar year, the lower the following spring's runoff efficiency will be (Figure 2b). This decreased efficiency may be the result of more of the following year's snowmelt going towards ET and less going to recharge groundwater and deep soil moisture storage, leading to drier conditions going into the following spring and a larger storage deficit that must be overcome before runoff is produced (Castillo

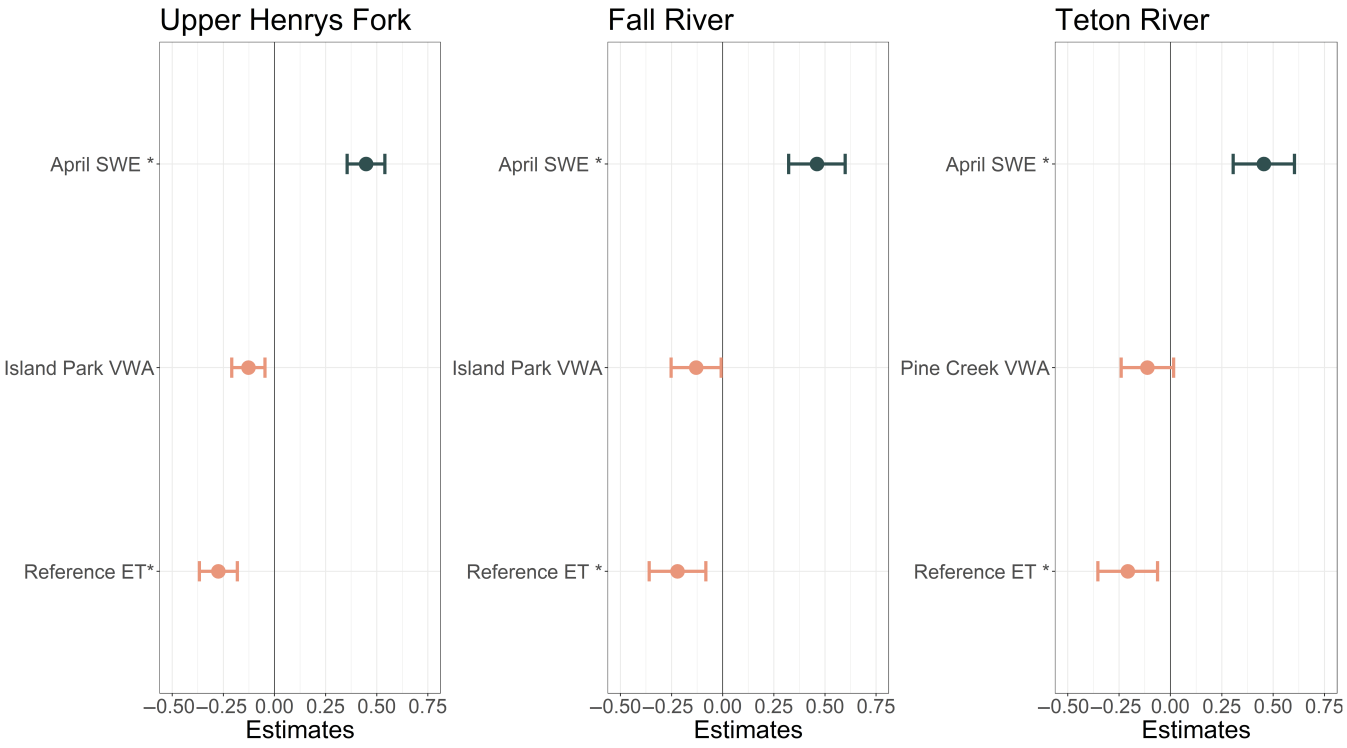

FIGURE 6 Standardized estimates of corrected Akaike's information criterion-selected seasonal predictive model coefficients. Asterisk following variable name indicates a log-transformed variable. Island Park and Pine Creek vegetation-water alignment (VWA) correspond to the VWA calculated at specific SNOTEL sites. Detailed description of each predictor is included in Table S1.

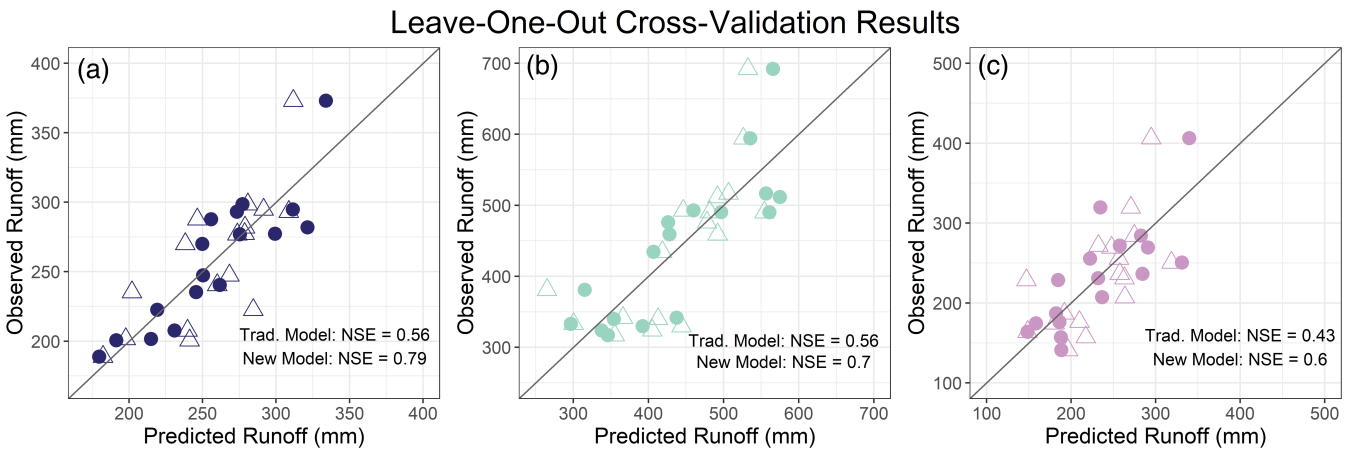

FIGURE 7 Predictive performance of new post-drought models from leave-one-out cross validation. Panels (a–c) shows the accuracy and Nash–Sutcliffe efficiency (NSE) of predicted versus observed runoff from the traditional model (open triangles) and new model (closed circle) for each watershed. Here, the 'traditional' model refers to a model fit with 1 April snow water equivalent and January runoff whereas the 'new' model refers to the Akaike's information criterion-selected best model for each watershed that is given in Figure 6.

et al., 2003; Harpold et al., 2017; McDonnell et al., 2021; Milly, 1994). By considering an extensive set of potential predictors during the new model selection, we see that when paired with ETr, VWA provided more predictive power than other commonly used metrics, including a one-year moving average mass balance deficit metric. Metrics that track accrued deficits and surpluses of precipitation and ET have been shown to improve runoff predictions following drought due to their ability to detect changes in root-zone storage deficits (Lapides et al., 2022; Wang-Erlandsson et al., 2016). Unlike many deficit metrics, the VWA does not require additional choices about temporal aggregation, and thus provides new insights by quantifying the synchrony of annual water inputs and vegetation greenness to capture spring snowmelt dynamics as well as dry season changes in NDVI that reflect vegetative stress that may be missed at coarser resolutions. The predictive power of mass balance deficit metrics, ETr and VWA, particularly after dry years, supports a conceptual model where spring

TABLE 1 Leave-one-out performance metrics of traditional and new models for the post-drought period by watershed.

Watershed	Model	NSE	PBIAS	$RMSE_{sd}$
Upper Henrys	Traditional	0.564	−0.308	0.640
	New	0.790	−0.129	0.447
Fall	Traditional	0.563	−0.642	0.641
	New	0.700	−0.427	0.534
Teton	Traditional	0.432	0.268	0.731
	New	0.601	−0.298	0.613

Abbreviations: NSE, Nash–Sutcliffe efficiency; PBIAS, percent bias; RMSE, root mean square error.

runoff occurs after storage deficits is refilled (McDonnell et al., 2021). The significance of this work goes beyond just a mechanistic understanding of streamflow generation; it also guides how we can integrate these processes into regression-based predictive models at the time scale needed for seasonal predictions.

In the context of the proposed mechanisms driving variable streamflow response to changes in snowpack, our results support the importance of capturing changes in energy-water synchrony (Gordon et al., 2022). While not explicitly modelling energy synchrony, the VWA indirectly accounts for spring and summer temperatures by using NDVI, which reflects the timing of snow disappearance, length of the growing season and provides inferences of ET without any of the assumptions often used in ET models, all of which reflect energy changes. Additionally, this metric also captures changes in the timing and magnitude of SWI inputs related to changes in melt rates, an important insight given that faster melt rates have been shown to produce larger streamflow responses (Barnhart et al., 2016, 2020).

4.3 | Variability in model performance between watersheds

The new models improved streamflow predictions the most in the Upper Henrys Fork (Figure 7). This improvement may be due to a combination of factors, including the groundwater-dominated hydrologic regime, greater forest regrowth following disturbance, and the watershed's topography. The Upper Henrys Fork is the only one of the three watersheds that has experienced both significant warming and higher $NDVI_{MAX}$ over both satellite periods of record (Figure 4). This suggests that, as expected, the more change a watershed has experienced, the greater the need to revise traditional predictive relationships. Compounding this change in the Upper Henrys Fork is the memory of past deficits retained in the groundwater system (Benjamin, 2000).

Groundwater-dominated systems experience a larger absolute reduction in summer streamflow following changes in snowmelt timing and warming than their snow-dominated counterparts (Mayer & Naman, 2011; Tague & Grant, 2009). This is especially true in porous, young volcanic landscapes (Tague et al., 2008), such as the calderas and tuffs that underly the Upper Henrys. Not only do deficits accrue due to the slower drainage rates but also these porous substrates may have a large subsurface storage capacity. This stored water can modulate the hydrologic impacts of climate–ET interactions if this water is accessible to plants during dry periods (Garcia & Tague, 2015; Klos et al., 2018). This increased storage allows plants to deplete deeper water stores during multi-year dry periods, resulting in lower streamflow generation and greater deficits (Hahm et al., 2020, 2022).

Improved predictive performance in Fall River, a watershed underlain by a mix of young volcanic and glacial deposits with a more mixed groundwater-snowmelt system, also supports the important role underlying geology and subsurface storage capacity may play in modulating runoff efficiency. Our analysis shows more moderate improvements in the snowmelt-dominated Teton River, perhaps indicative of the larger role of real-time melt dynamics in snowmelt-driven systems. The importance of capturing snowpack evolution and melt in near-real time has motivated efforts to operationalize physically based models to provide more accurate short-term forecasts (Meyer et al., 2023). However, these forecasts have much shorter lead times and depend on accurate meteorological forecasts, suggesting the value of also continuing to improve our understanding of snowmelt runoff efficiency on a seasonal scale.

In each new seasonal runoff model, SNOTEL sites in the low to intermediate elevation zones (1900–2100 m) were selected as the best predictors of streamflow (Figure 7). Previous work has shown that ET and vegetation greenness in intermediate elevation zones are more responsive to changes in annual precipitation and snowpack (Christensen et al., 2008; Kraft et al., 2022; Tague & Peng, 2013; Trujillo et al., 2012). This finding suggests that mid-elevation forests, which are able to optimally use available water, may exert a larger influence on storage deficits and runoff efficiency than forests that are more strongly water- or energy-limited. As warming shifts the timing between snowmelt and the growing season, annual and interannual hydrologic response will depend on how mid-elevation forests affect subsurface storage as they transition from energy- to water-limited growing seasons.

4.4 | Limitations and future work

This study provides a case study and proof of concept for the utility of the VWA, a new metric that captures changing vegetation dynamics and water-energy synchrony in improving seasonal runoff predictions. To demonstrate its utility, we focused on creating new models for the modern post-drought period, which extends back to 2006. This modern period of record allows us to use MODIS data without introducing additional uncertainty from relying on multiple satellite platforms and variable spatial and temporal resolutions; however, it reduces the period of record and does not record pre-drought or drought VWA values. Future work should look at the impact of temporal frequency and spatial resolution on the fit of the NDVI sine curves to try to extend the VWA record using AVHRR and Landsat data.

In this region, denser forests combined with warmer springs and summers set the scene for changing snow–vegetation interactions and greater evaporative demand to have a noticeable effect on local hydrology. Follow-up studies should investigate the utility of VWA in watersheds that have seen more widespread changes in snow accumulation and melt and/or recent vegetation disturbances. The similarity index of SWI and NDVI integrates many different aspects of snow-vegetation dynamics, and it would be valuable to investigate whether the effects a disturbance such as wildfire has on both SWI and NDVI translates to a meaningful shift in VWA that corresponds to a change in runoff efficiency.

5 | CONCLUSION

Here, we present a case study looking at how the relationships used in seasonal runoff predictive models have changed over the past three decades in the Henrys Fork of the Snake River, a forested headwater system located in the Greater Yellowstone Ecosystem. We see that predictive relationships used prior to a severe drought in the early 2000s over-predict runoff during and after the drought in two of the three watersheds, and that the remaining watershed shows declining performance in the post-drought period. Our analysis of climate and vegetation change over the same period shows that, although this region has not experienced widespread shifts in precipitation or snow accumulation since the late 1980s, late springs and summers are generally warmer and forests are greener with more tree-covered area as forests recover from multiple disturbances. These results suggest the changing snowpack–streamflow relationship is affected not just by changes in snow accumulation and melt, but also by vegetation dynamics, an aspect of watershed hydrology not historically captured in regression-based predictive models. To this end, we propose a new metric, the VWA, that quantifies water availability-growing season alignment. New predictive models show that this index, along with a metric of atmospheric demand, are significant predictors of runoff and can be used to improve the runoff predictions in the post-drought period. Furthermore, VWA for a given calendar year is a significant negative predictor of the following year's summer runoff. This supports the hypothesis that the more synchronized the timing of water inputs are with the growing season, the lower future runoff efficiency will be. This finding emphasizes that our understanding of runoff dynamics and our ability to predict runoff depends not only on our ability to model snowpack but also on our understanding of and ability to model how vegetation responds to warming and water stress and how these stress responses affect groundwater storage and recharge. The VWA proposed here is a step forward in integrating vegetation dynamics into seasonal predictive models and further work should be done to assess the applicability of this metric outside of the case study presented here.

ACKNOWLEDGEMENTS

We would like to thank the National Science Foundation (Award #1653998 & INTERN supplement) for project funding and the Henry's Fork Foundation for project resources. We would also like to thank Eva Jones and Christina Morrisett for insightful conversations and help with preliminary data analysis. We would also like to thank the three reviewers whose feedback improved this manuscript.

CONFLICT OF INTEREST STATEMENT

The authors declare no conflict of interest.

DATA AVAILABILITY STATEMENT

All data used here is publicly available from NRCS SNOTEL sites, MODIS Terra and Aqua satellites, USGS streamflow gages, and US Bureau of Reclamation AgriMet stations. Data and analysis scripts are submitted to HydroShare and accessible via http://www.hydroshare.org/resource/ff0280d1fe87494ca2f08e1f7c25ca41.

ORCID

Sarah K. Newcomb https://orcid.org/0000-0002-7832-5089
Sarah E. Godsey https://orcid.org/0000-0001-6529-7886
Maggi Kraft https://orcid.org/0000-0003-2649-4195

REFERENCES

Abatzoglou, J. T., & Williams, A. P. (2016). Impact of anthropogenic climate change on wildfire across western US forests. *Proceedings of the National Academy of Sciences*, *113*(42), 11770–11775. https://doi.org/10.1073/pnas.1607171113

Adams, H. D., Luce, C. H., Breshears, D. D., Allen, C. D., Weiler, M., Hale, V. C., Smith, A. M. S., & Huxman, T. E. (2012). Ecohydrological consequences of drought- and infestation-triggered tree die-off: Insights and hypotheses. *Ecohydrology*, *5*(2), 145–159. https://doi.org/10.1002/eco.233

Apurv, T., & Cai, X. (2020). Drought propagation in contiguous U.S. watersheds: A process-based understanding of the role of climate and watershed properties. *Water Resources Research*, *56*(9), e2020WR027755. https://doi.org/10.1029/2020WR027755

Atwood, J., Domonkos, B., Hill, K., Brosten, T., DeMarco, T., Hultstrand, M., Tappa, D., Austin, L., & Buckman, A. (2023). Evaluation of Ysi temperature correction equations for bias-reducing Snotel network temperature data. 2023 Western Snow Conference.

Avanzi, F., Rungee, J., Maurer, T., Bales, R., Ma, Q., Glaser, S., & Conklin, M. (2020). Climate elasticity of evapotranspiration shifts the water balance of Mediterranean climates during multi-year droughts. *Hydrology and Earth System Sciences*, *24*(9), 4317–4337. https://doi.org/10.5194/hess-24-4317-2020

Barnard, D. M., Green, T. R., Mankin, K. R., DeJonge, K. C., Rhoades, C. C., Kampf, S. K., Giovando, J., Wilkins, M. J., Mahood, A. L., Sears, M. G., Comas, L. H., Gleason, S. M., Zhang, H., Fassnacht, S. R., Harmel, R. D., & Altenhofen, J. (2023). Wildfire and climate change amplify knowledge gaps linking mountain source-water systems and agricultural water supply in the western United States. *Agricultural Water Management*, *286*, 108377. https://doi.org/10.1016/j.agwat.2023.108377

Barnett, T. P., Adam, J. C., & Lettenmaier, D. P. (2005). Potential impacts of a warming climate on water availability in snow-dominated regions. *Nature*, *438*(7066), 303–309. https://doi.org/10.1038/nature04141

Barnhart, T. B., Molotch, N. P., Livneh, B., Harpold, A. A., Knowles, J. F., & Schneider, D. (2016). Snowmelt rate dictates streamflow. *Geophysical Research Letters*, *43*(15), 8006–8016. https://doi.org/10.1002/2016GL069690

Barnhart, T. B., Tague, C. L., & Molotch, N. P. (2020). The counteracting effects of snowmelt rate and timing on runoff. *Water Resources*

Research, *56*(8), e2019WR026634. https://doi.org/10.1029/2019WR026634

Bartoń, K. (2023). _MuMIn: Multi-Model Inference_. R package version 1.47.5. https://CRAN.R-project.org/package=MuMIn

Benjamin, L. (2000). Groundwater hydrology of the Henry's Fork Springs. *Intermountain Journal of Sciences*, *6*(3), 119–142.

Berghuijs, W. R., Sivapalan, M., Woods, R. A., & Savenije, H. H. G. (2014). Patterns of similarity of seasonal water balances: A window into streamflow variability over a range of time scales. *Water Resources Research*, *50*(7), 5638–5661. https://doi.org/10.1002/2014WR015692

Berghuijs, W. R., & Woods, R. A. (2016). A simple framework to quantitatively describe monthly precipitation and temperature climatology. *International Journal of Climatology*, *36*(9), 3161–3174. https://doi.org/10.1002/joc.4544

Bonan, G. B. (2008). Forests and climate change: Forcings, feedbacks, and the climate benefits of forests. *Science*, *320*(5882), 1444–1449. https://doi.org/10.1126/science.1155121

Brooks, P. D., Gelderloos, A., Wolf, M. A., Jamison, L. R., Strong, C., Solomon, D. K., Bowen, G. J., Burian, S., Tai, X., Arens, S., Briefer, L., Kirkham, T., & Stewart, J. (2021). Groundwater-mediated memory of past climate controls water yield in snowmelt-dominated catchments. *Water Resources Research*, *57*(10), e2021WR030605. https://doi.org/10.1029/2021WR030605

Castillo, V. M., Gómez-Plaza, A., & Martínez-Mena, M. (2003). The role of antecedent soil water content in the runoff response of semiarid catchments: A simulation approach. *Journal of Hydrology*, *284*(1), 114–130. https://doi.org/10.1016/S0022-1694(03)00264-6

Cayan, D. R., Kammerdiener, S. A., Dettinger, M. D., Caprio, J. M., & Peterson, D. H. (2001). Changes in the onset of spring in the Western United States. *Bulletin of the American Meteorological Society*, *82*(3), 399–416. https://doi.org/10.1175/1520-0477(2001)082<0399:CITOOS>2.3.CO;2

Christensen, L., Adams, H. R., Tai, X., Barnard, H. R., & Brooks, P. D. (2021). Increasing plant water stress and decreasing summer streamflow in response to a warmer and wetter climate in seasonally snow-covered forests. *Ecohydrology*, *14*(1), e2256. https://doi.org/10.1002/eco.2256

Christensen, L., Tague, C. L., & Baron, J. S. (2008). Spatial patterns of simulated transpiration response to climate variability in a snow dominated mountain ecosystem. *Hydrological Processes*, *22*(18), 3576–3588. https://doi.org/10.1002/hyp.6961

Claeskens, G., & Hjort, N. L. (2008). *Model selection and model averaging (Cambridge books)*. Cambridge University Press. Retrieved from https://econpapers.repec.org/bookchap/cupcbooks/9780521852258.htm

Cooper, A. E., Kirchner, J. W., Wolf, S., Lombardozzi, D. L., Sullivan, B. W., Tyler, S. W., & Harpold, A. A. (2020). Snowmelt causes different limitations on transpiration in a Sierra Nevada conifer forest. *Agricultural and Forest Meteorology*, *291*, 108089. https://doi.org/10.1016/j.agrformet.2020.108089

Dai, A. (2013). Increasing drought under global warming in observations and models. *Nature Climate Change*, *3*(1), 52–58. https://doi.org/10.1038/nclimate1633

Dewitz, J. (2023). *National land cover database (NLCD) 2021 Products [Data set]*. U.S. Geological Survey. https://doi.org/10.5066/P9JZ7AO3

Dickerson-Lange, S. E., Vano, J. A., Gersonde, R., & Lundquist, J. D. (2021). Ranking forest effects on snow storage: A decision tool for Forest management. *Water Resources Research*, *57*(10), e2020WR027926. https://doi.org/10.1029/2020WR027926

Didan, K., Munoz, A. B., & Huete, A. (2015). *MODIS vegetation index user's guide* (MOD13 Series). The University of Arizona: Vegetation Index and Phenology Lab.

Elzhov, T. V., Mullen, K. M., Spiess, A., & Bolker, B. (2023). _minpack.lm: R Interface to the Levenberg-Marquardt Nonlinear Least-Squares Algorithm Found in MINPACK, Plus Support for Bounds_. R package version 1.2-3. https://CRAN.R-project.org/package=minpack.lm

Garcia, E. S., & Tague, C. L. (2015). Subsurface storage capacity influences climate–evapotranspiration interactions in three western United States catchments. *Hydrology and Earth System Sciences*, *19*(12), 4845–4858. https://doi.org/10.5194/hess-19-4845-2015

Garen, D. C. (1992). Improved techniques in regression-based streamflow volume forecasting. *Journal of Water Resources Planning and Management*, *118*(6), 654–670. https://doi.org/10.1061/(ASCE)0733-9496(1992)118:6(654)

Godsey, S. E., Kirchner, J. W., & Tague, C. L. (2014). Effects of changes in winter snowpacks on summer low flows: Case studies in the Sierra Nevada, California, USA. *Hydrological Processes*, *28*(19), 5048–5064. https://doi.org/10.1002/hyp.9943

Goeking, S. A., & Tarboton, D. G. (2020). Forests and water yield: A synthesis of disturbance effects on streamflow and snowpack in Western coniferous forests. *Journal of Forestry*, *118*(2), 172–192. https://doi.org/10.1093/jofore/fvz069

Goeking, S. A., & Tarboton, D. G. (2022). Variable streamflow response to forest disturbance in the Western US: A large-sample hydrology approach. *Water Resources Research*, *58*(6), e2021WR031575. https://doi.org/10.1029/2021WR031575

Gordon, B. L., Brooks, P. D., Krogh, S. A., Boisrame, G. F. S., Carroll, R. W. H., McNamara, J. P., & Harpold, A. A. (2022). Why does snowmelt-driven streamflow response to warming vary? A data-driven review and predictive framework. *Environmental Research Letters*, *17*(5), 053004. https://doi.org/10.1088/1748-9326/ac64b4

Goulden, M. L., Anderson, R. G., Bales, R. C., Kelly, A. E., Meadows, M., & Winston, G. C. (2012). Evapotranspiration along an elevation gradient in California's Sierra Nevada. *Journal of Geophysical Research: Biogeosciences*, *117*(G3), G03028. https://doi.org/10.1029/2012JG002027

Goulden, M. L., & Bales, R. C. (2014). Mountain runoff vulnerability to increased evapotranspiration with vegetation expansion. *Proceedings of the National Academy of Sciences*, *111*(39), 14071–14075. https://doi.org/10.1073/pnas.1319316111

Grogan, D. S., Burakowski, E. A., & Contosta, A. R. (2020). Snowmelt control on spring hydrology declines as the vernal window lengthens. *Environmental Research Letters*, *15*(11), 114040. https://doi.org/10.1088/1748-9326/abbd00

Hahm, W. J., Dralle, D. N., Sanders, M., Bryk, A. B., Fauria, K. E., Huang, M. H., Hudson-Rasmussen, B., Nelson, M. D., Pedrazas, M. A., Schmidt, L., Whiting, J., Dietrich, W. E., & Rempe, D. M. (2022). Bedrock vadose zone storage dynamics under extreme drought: Consequences for plant water availability, recharge, and runoff. *Water Resources Research*, *58*(4), e2021WR031781. https://doi.org/10.1029/2021WR031781

Hahm, W. J., Rempe, D. M., Dralle, D. N., Dawson, T. E., & Dietrich, W. E. (2020). Oak transpiration drawn from the weathered bedrock vadose zone in the summer dry season. *Water Resources Research*, *56*(11), e2020WR027419. https://doi.org/10.1029/2020WR027419

Hale, K. E., Jennings, K. S., Musselman, K. N., Livneh, B., & Molotch, N. P. (2023). Recent decreases in snow water storage in western North America. *Communications Earth & Environment*, *4*(1), 1–11. https://doi.org/10.1038/s43247-023-00751-3

Hall, D. K., & Riggs, G. A. (2007). Accuracy assessment of the MODIS snow products. *Hydrological Processes*, *21*(12), 1534–1547. https://doi.org/10.1002/hyp.6715

Hamlet, A. F., Mote, P. W., Clark, M. P., & Lettenmaier, D. P. (2007). Twentieth-century trends in runoff, evapotranspiration, and soil moisture in the Western United States. *Journal of Climate*, *20*(8), 1468–1486. https://doi.org/10.1175/JCLI4051.1

Hammond, J. C., Harpold, A. A., Weiss, S., & Kampf, S. K. (2019). Partitioning snowmelt and rainfall in the critical zone: Effects of climate type and soil properties. *Hydrology and Earth System Sciences*, *23*(9), 3553–3570. https://doi.org/10.5194/hess-23-3553-2019

Hammond, J. C., & Kampf, S. K. (2020). Subannual streamflow responses to rainfall and snowmelt inputs in snow-dominated watersheds of the Western United States. *Water Resources Research*, *56*(4), e2019WR026132. https://doi.org/10.1029/2019WR026132

Harpold, A. A., Sutcliffe, K., Clayton, J., Goodbody, A., & Vazquez, S. (2017). Does including soil moisture observations improve operational streamflow forecasts in snow-dominated watersheds? *JAWRA Journal of the American Water Resources Association*, *53*(1), 179–196. https://doi.org/10.1111/1752-1688.12490

He, M., Russo, M., & Anderson, M. (2016). Predictability of seasonal streamflow in a changing climate in the Sierra Nevada. *Climate*, *4*(4), 57. https://doi.org/10.3390/cli4040057

Helsel, D. R., Hirsch, R. M., Ryberg, K. R., Archfield, S. A., & Gilroy, E. J. (2020). Statistical methods in water resources (No. 4-A3). In *Techniques and methods*. U.S. Geological Survey. https://doi.org/10.3133/tm4A3

Hernandez, A. J., Healey, S. P., Huang, H., & Ramsey, R. D. (2018). Improved prediction of stream flow based on updating land cover maps with remotely sensed forest change detection. *Forests*, *9*(6), 317. https://doi.org/10.3390/f9060317

Holben, B. N. (1986). Characteristics of maximum-value composite images from temporal AVHRR data. *International Journal of Remote Sensing*, *7*(11), 1417–1434. https://doi.org/10.1080/01431168608948945

Hostetler, S., Whitlock, C., Shuman, B., Liefert, D., Drimal, C. W., & Bischke, S. (2021). Greater yellowstone climate assessment: Past, present, and future climate change in greater yellowstone watersheds (technical report). Montana State University, Institute on Ecosystems. Retrieved from https://scholarworks.montana.edu/xmlui/handle/1/16361

Huang, S., Tang, L., Hupy, J. P., Wang, Y., & Shao, G. (2021). A commentary review on the use of normalized difference vegetation index (NDVI) in the era of popular remote sensing. *Journal of Forestry Research*, *32*(1), 1–6. https://doi.org/10.1007/s11676-020-01155-1

Huntington, J. L., Hegewisch, K. C., Daudert, B., Morton, C. G., Abatzoglou, J. T., McEvoy, D. J., & Erickson, T. (2017). Climate engine: Cloud computing and visualization of climate and remote sensing data for advanced natural resource monitoring and process understanding. *Bulletin of the American Meteorological Society*, *98*(11), 2397–2410. https://doi.org/10.1175/BAMS-D-15-00324.1

Hwang, T., Martin, K. L., Vose, J. M., Wear, D., Miles, B., Kim, Y., & Band, L. E. (2018). Nonstationary hydrologic behavior in forested watersheds is mediated by climate-induced changes in growing season length and subsequent vegetation growth. *Water Resources Research*, *54*(8), 5359–5375. https://doi.org/10.1029/2017WR022279

Idaho Water Resources Board. (2009). Eastern snake plain aquifer. *Boise: Comprehensive Aquifer Management Plan*, 31.

Jennings, K. S., & Molotch, N. P. (2019). The sensitivity of modeled snow accumulation and melt to precipitation phase methods across a climatic gradient. *Hydrology and Earth System Sciences*, *23*(9), 3765–3786. https://doi.org/10.5194/hess-23-3765-2019

Jin, S., & Sader, S. A. (2005). MODIS time-series imagery for forest disturbance detection and quantification of patch size effects. *Remote Sensing of Environment*, *99*(4), 462–470. https://doi.org/10.1016/j.rse.2005.09.017

Klos, P. Z., Goulden, M. L., Riebe, C. S., Tague, C. L., O'Geen, A. T., Flinchum, B. A., Khan, S., Conklin, M. H., Hart, S. C., Berhe, A. A., Hartsough, P., Holbrook, S., & Bales, R. C. (2018). Subsurface plant-accessible water in mountain ecosystems with a Mediterranean climate. *WIREs Water*, *5*(3), e1277. https://doi.org/10.1002/wat2.1277

Klos, P. Z., Link, T. E., & Abatzoglou, J. T. (2014). Extent of the rain-snow transition zone in the western U.S. under historic and projected climate. *Geophysical Research Letters*, *41*(13), 4560–4568. https://doi.org/10.1002/2014GL060500

Knighton, J., Vijay, V., & Palmer, M. (2020). Alignment of tree phenology and climate seasonality influences the runoff response to forest cover loss. *Environmental Research Letters*, *15*(10), 104051. https://doi.org/10.1088/1748-9326/abaad9

Kormos, P. R., Marks, D., McNamara, J. P., Marshall, H. P., Winstral, A., & Flores, A. N. (2014). Snow distribution, melt and surface water inputs to the soil in the mountain rain–snow transition zone. *Journal of Hydrology*, *519*, 190–204. https://doi.org/10.1016/j.jhydrol.2014.06.051

Koster, R. D., Mahanama, S. P. P., Livneh, B., Lettenmaier, D. P., & Reichle, R. H. (2010). Skill in streamflow forecasts derived from large-scale estimates of soil moisture and snow. *Nature Geoscience*, *3*(9), 613–616. https://doi.org/10.1038/ngeo944

Kottek, M., Grieser, J., Beck, C., Rudolf, B., & Rubel, F. (2006). World map of the Köppen-Geiger climate classification updated. *Meteorologische Zeitschrift*, *15*, 259–263. https://doi.org/10.1127/0941-2948/2006/0130

Kraft, M., & McNamara, J. P. (2022). Evapotranspiration across the rain–snow transition in a semi-arid watershed. *Hydrological Processes*, *36*(3), e14519. https://doi.org/10.1002/hyp.14519

Kraft, M., McNamara, J. P., Marshall, H.-P., & Glenn, N. F. (2022). Forest impacts on snow accumulation and melt in a semi-arid mountain environment. *Frontiers in Water*, *4*, 1004123. https://doi.org/10.3389/frwa.2022.1004123

Lapides, D. A., Hahm, W. J., Rempe, D. M., Whiting, J., & Dralle, D. N. (2022). Causes of missing snowmelt following drought. *Geophysical Research Letters*, *49*(19), e2022GL100505. https://doi.org/10.1029/2022GL100505

Lawler, R. R., & Link, T. E. (2011). Quantification of incoming all-wave radiation in discontinuous forest canopies with application to snowmelt prediction. *Hydrological Processes*, *25*(21), 3322–3331. https://doi.org/10.1002/hyp.8150

Li, D., Wrzesien, M. L., Durand, M., Adam, J., & Lettenmaier, D. P. (2017). How much runoff originates as snow in the western United States, and how will that change in the future? *Geophysical Research Letters*, *44*(12), 6163–6172. https://doi.org/10.1002/2017GL073551

Lilliefors, H. W. (1967). On the Kolmogorov-Smirnov test for normality with mean and variance unknown. *Journal of the American Statistical Association*, *62*(318), 399–402. https://doi.org/10.1080/01621459.1967.10482916

Livneh, B., & Badger, A. M. (2020). Drought less predictable under declining future snowpack. *Nature Climate Change*, *10*(5), 452–458. https://doi.org/10.1038/s41558-020-0754-8

Lundquist, J. D., Dickerson-Lange, S. E., Lutz, J. A., & Cristea, N. C. (2013). Lower forest density enhances snow retention in regions with warmer winters: A global framework developed from plot-scale observations and modeling. *Water Resources Research*, *49*(10), 6356–6370. https://doi.org/10.1002/wrcr.20504

Manning, A. L., Harpold, A., & Csank, A. (2022). Spruce beetle outbreak increases streamflow from snow-dominated basins in Southwest Colorado, USA. *Water Resources Research*, *58*(5), e2021WR029964. https://doi.org/10.1029/2021WR029964

Martínez-Vilalta, J., & Garcia-Forner, N. (2017). Water potential regulation, stomatal behaviour and hydraulic transport under drought: Deconstructing the iso/anisohydric concept. *Plant, Cell & Environment*, *40*(6), 962–976. https://doi.org/10.1111/pce.12846

Massmann, A., Gentine, P., & Lin, C. (2019). When does vapor pressure deficit drive or reduce evapotranspiration? *Journal of Advances in Modeling Earth Systems*, *11*(10), 3305–3320. https://doi.org/10.1029/2019MS001790

Maurer, T., Avanzi, F., Glaser, S. D., & Bales, R. C. (2022). Drivers of drought-induced shifts in the water balance through a Budyko approach. *Hydrology and Earth System Sciences*, *26*(3), 589–607. https://doi.org/10.5194/hess-26-589-2022

Mayer, T. D., & Naman, S. W. (2011). Streamflow response to climate as influenced by geology and elevation†. *JAWRA Journal of the American Water Resources Association*, *47*(4), 724–738. https://doi.org/10.1111/j.1752-1688.2011.00537.x

McDonnell, J. J., Spence, C., Karran, D. J., van Meerveld (Ilja), H. J., & Harman, C. J. (2021). Fill-and-spill: A process description of runoff generation at the scale of the beholder. *Water Resources Research*, *57*(5), e2020WR027514. https://doi.org/10.1029/2020WR027514

McLeod, A. (2022). _Kendall: Kendall Rank Correlation and Mann-Kendall Trend Test_. R package version 2.2.1. https://CRAN.R-project.org/package=Kendall

Melcher, N. B., & Walker, J. F. (1992). *Evaluation of selected methods for determining streamflow during periods of ice effect* (No. 2378). Water supply paper. U.S. Geological Survey. https://doi.org/10.3133/wsp2378

Mendoza, P. A., Wood, A. W., Clark, E., Rothwell, E., Clark, M. P., Nijssen, B., Brekke, L. D., & Arnold, J. R. (2017). An intercomparison of approaches for improving operational seasonal streamflow forecasts. *Hydrology and Earth System Sciences*, *21*(7), 3915–3935. https://doi.org/10.5194/hess-21-3915-2017

Meyer, J., Horel, J., Kormos, P., Hedrick, A., Trujillo, E., & Skiles, S. M. (2023). Operational water forecast ability of the HRRR-iSnobal combination: An evaluation to adapt into production environments. *Geoscientific Model Development*, *16*(1), 233–250. https://doi.org/10.5194/gmd-16-233-2023

Milly, P. C. D. (1994). Climate, soil water storage, and the average annual water balance. *Water Resources Research*, *30*(7), 2143–2156. https://doi.org/10.1029/94WR00586

Montesi, J., Elder, K., Schmidt, R. A., & Davis, R. E. (2004). Sublimation of intercepted snow within a subalpine forest canopy at two elevations. *Journal of Hydrometeorology*, *5*(5), 763–773. https://doi.org/10.1175/1525-7541(2004)005<0763:SOISWA>2.0.CO;2

Moriasi, D. N., Arnold, J. G., Van Liew, M. W., Bingner, R. L., Harmel, R. D., & Veith, T. L. (2007). Model evaluation guidelines for systematic quantification of accuracy in watershed simulations. *Transactions of the ASABE*, *50*(3), 885–900. https://doi.org/10.13031/2013.23153

Morrisett, C. N., Van Kirk, R. W., & Null, S. E. (2023). Assessing downstream aquatic habitat availability relative to headwater reservoir management in the henrys fork snake river. *River Research and Applications*, *39*(9), 1749–1762. https://doi.org/10.1002/rra.4175

Mote, P. W., Li, S., Lettenmaier, D. P., Xiao, M., & Engel, R. (2018). Dramatic declines in snowpack in the western US. *npj Climate and Atmospheric Science*, *1*(1), 1–6. https://doi.org/10.1038/s41612-018-0012-1

Musselman, K. N., Clark, M. P., Liu, C., Ikeda, K., & Rasmussen, R. (2017). Slower snowmelt in a warmer world. *Nature Climate Change*, *7*(3), 214–219. https://doi.org/10.1038/nclimate3225

Musselman, K. N., Molotch, N. P., Margulis, S. A., Kirchner, P. B., & Bales, R. C. (2012). Influence of canopy structure and direct beam solar irradiance on snowmelt rates in a mixed conifer forest. *Agricultural and Forest Meteorology*, *161*, 46–56. https://doi.org/10.1016/j.agrformet.2012.03.011

Pagano, T., Garen, D., & Sorooshian, S. (2004). Evaluation of official Western U.S. seasonal water supply outlooks, 1922–2002. *Journal of Hydrometeorology*, *5*(5), 896–909. https://doi.org/10.1175/1525-7541(2004)005<0896:EOOWUS>2.0.CO;2

Patakamuri, S., & O'Brien, N. (2021). _modifiedmk: Modified Versions of Mann Kendall and Spearman's Rho Trend Tests_. R package version 1.6. https://CRAN.R-project.org/package=modifiedmk

Pepin, N., Bradley, R. S., Diaz, H. F., Baraer, M., Caceres, E. B., Forsythe, N., Fowler, H. J., Greenwood, G., Hashmi, M. Z. u. R., Liu, X. D., Miller, J. R., Ning, L., Ohmura, A., Palazzi, E., Rangwala, I., Schöner, W., Severskiy, I., Shahgedanova, M., Wang, M. B., … Yang, D. (2015). Elevation-dependent warming in mountain regions of the world. *Nature Climate Change*, *5*(5), 424–430. https://doi.org/10.1038/nclimate2563

Peterson, T. J., Saft, M., Peel, M. C., & John, A. (2021). Watersheds may not recover from drought. *Science*, *372*(6543), 745–749. https://doi.org/10.1126/science.abd5085

Pierce, K., Despain, D., Morgan, L., & Good, J. (2007). *The yellowstone hotspot, greater yellowstone ecosystem, and human geography*. Publications of the US Geological Survey. Retrieved from https://digitalcommons.unl.edu/usgspubs/79

Pierce, K. L., & Morgan, L. A. (1992). Chapter 1: The track of the yellowstone hot spot: Volcanism, faulting, and uplift. In P. K. Link, M. A. Kuntz, & L. B. Piatt (Eds.), *Regional geology of eastern Idaho and Western Wyoming* (Vol. 179). Geological Society of America. https://doi.org/10.1130/MEM179-p1

Potter, N. J., Zhang, L., Milly, P. C. D., McMahon, T. A., & Jakeman, A. J. (2005). Effects of rainfall seasonality and soil moisture capacity on mean annual water balance for Australian catchments. *Water Resources Research*, *41*(6), W06007. https://doi.org/10.1029/2004WR003697

Rigge, M. B., Bunde, B., Shi, H., & Postma, K. (2021). *Rangeland condition monitoring assessment and projection (RCMAP) fractional component time-series across the Western U.S. 1985–2020 [Data set]*. U.S. Geological Survey. https://doi.org/10.5066/P95IQ4BT

Robles, M. D., Hammond, J. C., Kampf, S. K., Biederman, J. A., & Demaria, E. M. C. (2021). Winter inputs buffer streamflow sensitivity to snowpack losses in the salt river watershed in the lower Colorado river basin. *Water*, *13*(1), 3. https://doi.org/10.3390/w13010003

Ryan, K. C., & Amman, G. D. (1996). *Bark beetle activity and delayed tree mortality in the greater yellowstone area following the 1988 fires*. International Association Wildland Fire.

Saft, M., Western, A. W., Zhang, L., Peel, M. C., & Potter, N. J. (2015). The influence of multiyear drought on the annual rainfall-runoff relationship: An Australian perspective. *Water Resources Research*, *51*(4), 2444–2463. https://doi.org/10.1002/2014WR015348

Seidl, R., Thom, D., Kautz, M., Martin-Benito, D., Peltoniemi, M., Vacchiano, G., Wild, J., Ascoli, D., Petr, M., Honkaniemi, J., Lexer, M. J., Trotsiuk, V., Mairota, P., Svoboda, M., Fabrika, M., Nagel, T. A., & Reyer, C. P. O. (2017). Forest disturbances under climate change. *Nature Climate Change*, *7*(6), 395–402. https://doi.org/10.1038/nclimate3303

Sexstone, G. A., Clow, D. W., Fassnacht, S. R., Liston, G. E., Hiemstra, C. A., Knowles, J. F., & Penn, C. A. (2018). Snow sublimation in mountain environments and its sensitivity to forest disturbance and climate warming. *Water Resources Research*, *54*(2), 1191–1211. https://doi.org/10.1002/2017WR021172

Stewart, I. T., Cayan, D. R., & Dettinger, M. D. (2005). Changes toward earlier streamflow timing across Western North America. *Journal of Climate*, *18*(8), 1136–1155. https://doi.org/10.1175/JCLI3321.1

Sun, A. Y., Wang, D., & Xu, X. (2014). Monthly streamflow forecasting using gaussian process regression. *Journal of Hydrology*, *511*, 72–81. https://doi.org/10.1016/j.jhydrol.2014.01.023

Tague, C., Grant, G., Farrell, M., Choate, J., & Jefferson, A. (2008). Deep groundwater mediates streamflow response to climate warming in the Oregon cascades. *Climatic Change*, *86*(1), 189–210. https://doi.org/10.1007/s10584-007-9294-8

Tague, C., & Grant, G. E. (2009). Groundwater dynamics mediate low-flow response to global warming in snow-dominated alpine regions. *Water Resources Research*, *45*(7), 7421. https://doi.org/10.1029/2008WR007179

Tague, C., & Peng, H. (2013). The sensitivity of forest water use to the timing of precipitation and snowmelt recharge in the California Sierra: Implications for a warming climate. *Journal of Geophysical Research: Biogeosciences*, *118*(2), 875–887. https://doi.org/10.1002/jgrg.20073

Tewari, S., Kulhavý, J., Bn, R., & Hadaš, P. (2012). Remote monitoring of forest response to changed soil moisture regime due to river regulation. *Journal of Forest Science*, *49*(9), 429–438. https://doi.org/10.17221/4716-JFS

Tian, W., Liu, X., Liu, C., & Bai, P. (2018). Investigation and simulations of changes in the relationship of precipitation-runoff in drought years. *Journal of Hydrology*, *565*, 95–105. https://doi.org/10.1016/j.jhydrol.2018.08.015

Trujillo, E., Molotch, N., Goulden, M., Kelly, A., & Bales, R. (2012). Elevation-dependent influence of snow accumulation on forest greening. *Nature Geoscience*, *5*, 705–709. https://doi.org/10.1038/ngeo1571

Turner, M. G., Romme, W. H., & Tinker, D. B. (2003). Surprises and lessons from the 1988 yellowstone fires. *Frontiers in Ecology and the Environment*, *1*(7), 351–358. https://doi.org/10.1890/1540-9295(2003)001[0351:SALFTY]2.0.CO;2

U.S. Bureau of Reclamation and Idaho Water Resource Board. (2015). Henrys Fork Basin Study final report.

Van Kirk, R. W. (2020). Analysis of water balance in the Henry's fork watershed. *Henry's Fork Foundation*, 1–23. https://www.henrysfork.org/_files/ugd/650d73_71607a75369f4f9fa8c618086240cfc5.pdf

Van Kirk, R. W., Hoffner, B., Verbeten, A., & Yates, S. (2019). New approaches to providing streamflow for fisheries in the American west: Embracing prior appropriation and the marketplace. In D. C. Dauwalter, T. W. Birdsong, & G. P. Garrett (Eds.), *Multispecies and watershed approaches in freshwater conservation* (pp. 515–564). American Fisheries Society.

van Leeuwen, W. J. D., Orr, B. J., Marsh, S. E., & Herrmann, S. M. (2006). Multi-sensor NDVI data continuity: Uncertainties and implications for vegetation monitoring applications. *Remote Sensing of Environment*, *100*(1), 67–81. https://doi.org/10.1016/j.rse.2005.10.002

Vano, J. A. (2020). Implications of losing snowpack. *Nature Climate Change*, *10*(5), 388–390. https://doi.org/10.1038/s41558-020-0769-1

Wang, T., Peng, S., Lin, X., & Chang, J. (2013). Declining snow cover may affect spring phenological trend on the Tibetan plateau. *Proceedings of the National Academy of Sciences*, *110*(31), E2854–E2855. https://doi.org/10.1073/pnas.1306157110

Wang-Erlandsson, L., Bastiaanssen, W. G. M., Gao, H., Jägermeyr, J., Senay, G. B., van Dijk, A. I. J. M., Guerschman, J. P., Keys, P. W., Gordon, L. J., & Savenije, H. H. G. (2016). Global root zone storage capacity from satellite-based evaporation. *Hydrology and Earth System Sciences*, *20*(4), 1459–1481. https://doi.org/10.5194/hess-20-1459-2016

White, M. A., De Beurs, K. M., Didan, K., Inouye, D. W., Richardson, A. D., Jensen, O. P., O'Keefe, J., Zhang, G., Nemani, R., Van Leeuwen, W. J. D., Brown, J. F., De Wit, A., Schaepman, M., Lin, X., Dettinger, M. D., Bailey, A. S., Kimball, J. S., Schwartz, M. D., Baldocchi, D., … Lauenroth, W. K. (2009). Intercomparison, interpretation, and assessment of spring phenology in North America estimated from remote sensing for 1982–2006. *Global Change Biology*, *15*(10), 2335–2359. https://doi.org/10.1111/j.1365-2486.2009.01910.x

Woods, R. A. (2009). Analytical model of seasonal climate impacts on snow hydrology: Continuous snowpacks. *Advances in Water Resources*, *32*(10), 1465–1481. https://doi.org/10.1016/j.advwatres.2009.06.011

Zhang, Y., Song, C., Band, L. E., Sun, G., & Li, J. (2017). Reanalysis of global terrestrial vegetation trends from MODIS products: Browning or greening? *Remote Sensing of Environment*, *191*, 145–155. https://doi.org/10.1016/j.rse.2016.12.018

Zhao, F., Zhang, L., Xu, Z., & Scott, D. F. (2010). Evaluation of methods for estimating the effects of vegetation change and climate variability on streamflow. *Water Resources Research*, *46*(3), W03505. https://doi.org/10.1029/2009WR007702

SUPPORTING INFORMATION

Additional supporting information can be found online in the Supporting Information section at the end of this article.

How to cite this article: Newcomb, S. K., Van Kirk, R. W., Godsey, S. E., & Kraft, M. (2024). Alignment between water inputs and vegetation green-up reduces next year's runoff efficiency. *Hydrological Processes*, *38*(6), e15211. https://doi.org/10.1002/hyp.15211